AN ABSTRACT OF THE THESIS OF

Erin K. Peck for the degree of Master of Science in Ocean, Earth, and Atmospheric Sciences presented on April 25, 2017.

Title: Competing Roles of Sea Level Rise and Sediment Supply on Sediment Accretion and Carbon Burial in Tidal Wetlands; Northern Oregon, U.S.A.

Abstract approved:

_____

Robert A. Wheatcroft

Quantification of contemporary sediment and carbon accumulation within Oregon tidal saline wetlands will: (1) fill a critical knowledge gap, and (2) naturally test without complicating variables whether sea level rise or sediment supply primarily control wetland growth. Here we measure vertical accretion rates and carbon burial rates in three Oregon estuaries – Youngs Bay, Tillamook Bay, and the Salmon River Estuary – of differing relative sea level rise rates (0.28 ± 0.44, 1.8 ± 0.4, and 2.2 ± 0.3 mm yr^{-1}, respectively) and sediment loads (39, 160, and 24 t yr^{-1}, respectively). Tillamook Bay and the Salmon River Estuary, which have similar rates of sea level rise but vastly different sediment loads, are accreting comparably (2.2 ± 0.3 and 2.4 ± 0.7 mm yr^{-1}, respectively), indicating the importance of rising sea level and increased hydroperiod. Youngs Bay, with the lowest rate of sea level rise and a moderate sediment supply, is accreting the quickest (2.7 ± 0.6 mm yr^{-1}) suggesting the tidal wetlands are either not in steady state with sea level rise or suspended sediment may be higher in this estuary. Mean vertical accretion within the three estuaries is greater than sea level rise, all

systems appear to have an excess of sediment, and Youngs Bay and Tillamook Bay exhibit rapidly accreting locations; therefore, despite many of these wetland's inability to migrate landward, they will likely keep pace with projections of accelerated sea level rise over the coming century. Additionally, though the mean rates of carbon burial in these Oregon wetlands are about half the global average (94 ± 33 g C_{org} m^{-2} yr^{-1}), carbon accretion is dictated by vertical accretion which will increase under imminent sea level rise.

Competing Roles of Sea Level Rise and Sediment Supply on Sediment Accretion and Carbon Burial in Tidal Wetlands; Northern Oregon, U.S.A.

by

Erin K. Peck

A THESIS

submitted to

Oregon State University

in partial fulfillment of
the requirements for the
degree of

Master of Science

Presented April 25, 2017
Commencement June 2017

Master of Science thesis of Erin K. Peck presented on April 25, 2017

APPROVED:

Major Professor, representing Ocean, Earth, & Atmospheric Sciences

Dean of the College of Earth, Ocean, and Atmospheric Sciences

Dean of the Graduate School

I understand that my thesis will become part of the permanent collection of Oregon State University libraries. My signature below authorizes release of my thesis to any reader upon request.

Erin K. Peck, Author

ACKNOWLEDGEMENTS

I find myself indebted foremost to my advisor, Rob Wheatcroft, for his tireless guidance and support within the field, laboratory, and office. Without his mentorship, this project would not have been possible and the quality of my Master of Science degree would have been much diminished. I am also immensely appreciative of Laura Brophy's boundless knowledge of Oregon's estuaries, generous help in the field, and musings on tidal wetland processes. Laura was additionally responsible for much of this project's financial support as the data presented here was originally collected for two restoration monitoring projects within Youngs Bay (Wallooskee Youngs restoration site) and Tillamook Bay (Southern Flow Corridor restoration site). Laura, working with the Institute for Applied Ecology, procured funding for the Youngs Bay and Tillamook Bay projects through the Bonneville Power Administration and U.S. Fish and Wildlife Service; and the National Oceanic and Atmospheric Administration, Oregon Watershed Enhancement Board, and U.S. Fish and Wildlife Service, respectively. Oregon SeaGrant has been an additional funder of this research. I would also like to thank Miguel Goñi for allowing me use of his lab in processing samples for organic carbon analysis and for advice throughout this procedure. Cynthia Sellinger has been a kind graduate committee representative, expressing sincere interest in my research and success as a graduate student. Lastly, I would like to express my deepest appreciation to the volunteers that helped collect cores in the field, to those who have guided me on laboratory procedures and with data analysis, and to my friends and family.

TABLE OF CONTENTS

TABLE OF CONTENTS (Continued)

LIST OF FIGURES

LIST OF TABLES

1. Introduction

Tidal wetlands maintain high biotic diversity and primary productivity (Beck et al. 2001); influence many biogeochemical cycles as a critical junction between terrestrial and marine environments (Turner and Millward 2002); and are considered some of the most economically valuable ecosystems on the planet (Barbier et al. 2011). Despite their clear importance, a substantial number of U.S. estuaries – especially those along the Pacific Coast – are poorly studied. Oregon tidal wetlands like most other Pacific Northwest (PNW) wetlands are particularly underrepresented within literature concerning global wetland change (e.g., Chmura et al. 2003; Ouyang and Lee 2014; Crosby et al. 2016; Morris et al. 2016; Kirwan et al. 2016). The paucity of data on Oregon wetlands is likely attributable to their small size; excepting the Columbia River estuary, the median area of the major estuaries in Oregon is 11.3 km^2. However, Oregon estuaries provide economically and societally important ecosystem services. For instance, coastal upwelling during the summer combined with runoff from red-alder-dominated watersheds naturally enhances nutrients within Oregon estuaries leading to high productivity (Brown and Ozretich 2009). This enhanced productivity supports higher trophic levels and additionally may result in greater carbon burial within estuarine sediments. Though carbon burial in PNW tidal wetlands may be relatively high on a per-area basis (Crooks et al. 2014), small spatial extents limit the importance of Oregon tidal wetlands in global carbon budgets. Nevertheless, accurate assessment of carbon burial will help policy makers better establish the monetary value in carbon markets of tidal wetland protection and restoration. Salmon, which utilize estuarine productivity and tidal wetland habitat, remain a huge economic and cultural staple for the PNW, as well (Wissmar and Simenstad 1998). Runoff of eroded sediment from logging; pesticides, herbicides, fertilizers, and animal waste from

agriculture; and industrial pollutants and municipal solid waste from urban areas is trapped within and biogeochemically filtered by estuarine sediments (Thom and Borde 1998).

Astoundingly, an estimated 50% of tidal wetlands has been lost or damaged globally (Barbier et al. 2011), and another 20% to 45% (by area) is projected to be drowned by 2100 under the Intergovernmental Panel on Climate Change's (IPCC) mean and maximum estimates of eustatic sea level (ESL) rise (Craft et al. 2009). Further, the most notable cases of tidal wetland drowning are linked to limited sediment inputs (e.g., Mississippi River Delta, Chesapeake Bay, and Venice Lagoon; Weston 2014). However, national wetland aerial extents were considered stable by a 2004 – 2009 study (Dahl and Stedman 2013) and non-linear ecogeomorphic feedbacks may dampen the effects of accelerated ESL rise (French 2006). Briefly, sea level rise creates accommodation space for allochthonous sediment to accumulate while wetland vegetation thickens shoots adding organic matter (OM) at the surface and subsurface; this gained elevation is maintained through reduced current and wave speeds (Kirwan and Megonigal 2013). Bias within the literature towards reporting predominantly on threatened tidal wetlands has therefore led to an over-exaggeration of wetland vulnerability to future relative sea level (RSL) acceleration (Kirwan et al. 2016). Oregon wetlands provide contrasting examples, as they may be comparatively resilient. For instance, the Oregon coastline experiences both slow RSL rise and large quantities of sediment input, suggesting enhanced stability under these stressors. PNW estuaries are also relatively undisturbed in comparison to U.S. East and Gulf coast wetlands, experiencing only moderate exploitation since the 1800s, including diking for agriculture, dam construction, and increased erosion from logging (Thom and Borde 1998). In fact, most Oregon tidal wetland restoration projects simply require removal of dikes without extensive fill removal (Frenkel and

Morlan 1991) or relocation of residents as would be necessary in more populated estuaries (e.g., San Francisco Bay; Gedan et al. 2009). Despite these advantages, PNW estuaries may still be vulnerable to drowning as they are narrow and thus incapable of landward migration beyond the Coast Range foothills (Thom 1992). Many authors have identified areas susceptible to "coastal squeeze" as the most defenseless against drowning (Torio and Chmura 2013; Kirwan et al. 2016). Assessment of the current tidal wetland health, including vertical accretion rates under recent ESL rise and relative contributions of lithogenic sediment and organic carbon to accretion, within Oregon estuaries is thus imperative if we are to develop a baseline for ecosystem function, make global comparisons with PNW wetlands, and assess future resilience. Furthermore, ignoring Oregon wetlands may deprive us of an ideal field laboratory to test model predictions of wetland evolution, deemed integral by Mudd (2011).

RSL change has traditionally been thought to control the formation and evolution of tidal wetlands (Friedrichs and Perry 2001). As RSL rises creating accommodation space, the wetland platform aggrades vertically through feedbacks between the vegetation, sediment, and estuarine flow field, thereby maintaining position relative to sea level. However, recent studies have indicated that changes in sediment delivery rates may have largely determined the behavior of estuaries along the Atlantic and Gulf coasts of North America (e.g., Colman and Bratton 2003; Day et al. 2000; Kirwan et al. 2011). For example, in the Plum Island estuary, accelerated downstream sediment delivery due to erosion associated with land-use change following European settlement expanded tidal wetlands, while ecogeomorphic feedbacks maintained estuarine morphology after sediment supply was reduced in the 20th century (Kirwan et al. 2011). Wetland vegetation largely contributes to these feedbacks through addition of OM at the surface, decay and

subsequent expansion of subsurface OM, and reduction of current and wave speeds thus increasing sediment deposition and retention (Kirwan and Megonigal 2013). Consequently, the dominant factor – RSL rise or sediment delivery rate – controlling their formation and growth remains debated. This uncertainty is due mainly to confounding variables making comparisons within and amongst tidal wetlands difficult.

PNW estuaries present a unique opportunity to constrain the relative impacts of sea level change and sediment delivery rates over the past ~ 150 yrs because both factors vary along the coast, but in understood ways. Vertical land motions at the Oregon coast result from the large-scale subduction of the Juan de Fuca plate underneath the North American plate, and trench-parallel differences in strain accumulation cause latitudinally varying uplift rates (Mitchell et al. 1994). ESL rise in the Northeast Pacific Ocean coupled with this variable uplift results in a range of RSL changes between -1.0 mm y^{-1} in southern and northern Oregon (i.e., falling RSL), and +1.5 mm yr^{-1} in central Oregon (Komar et al. 2011). Independently, there exists a more than thirty-fold range in fluvial sediment flux to Oregon estuaries (Wheatcroft and Sommerfield 2005). Secondary variables, including tidal range, water temperature and salinity, particulate organic carbon (C_{org}) type, and wetland plant assemblages, remain relatively uniform within these estuaries, acting as controlled variables (Hickey and Banas 2003). Thus, we hypothesize that if vertical accretion rates reflect RSL change within three Oregon estuaries – Youngs Bay, Tillamook Bay, and the Salmon River estuary – despite vastly different sediment supplies, then RSL primarily controls wetland growth. However, we might conclude that the magnitude of sediment supply controls vertical accretion if these rates vary with sediment flux rather than RSL.

In summary, the goals of this study are four-fold:

1. Assess the relative importance of contemporary RSL change and the magnitude of sediment supply on tidal wetland vertical accretion within three estuaries that maintain differences among these primary variables but have similar secondary variables
2. Determine baseline characteristics such as carbon burial and vertical accretion to assist other researchers and coastal management planners
3. Better place PNW tidal wetlands within global assessments of ecosystem services and vulnerability to climate change and human impacts
4. Make predictions about Oregon tidal wetland resilience in light of accelerated ESL rise and changes in fluvial sediment load

2. Study area and methods

2.1 Study sites

All three estuaries – Youngs Bay, Tillamook Bay, and the Salmon River Estuary – are located on the northern coast of Oregon (Figure 1A). The Youngs and Lewis and Clark Rivers drain the 478 km^2 Youngs Bay watershed (Figure 1B). The Youngs River, along which core sites were located, drains the largest portion of the watershed, 319 km^2. The estuary exchanges water with the much larger Columbia River Estuary through its 3.7-km-wide inlet. The U.S. National Oceanic and Atmospheric Administration (NOAA) report semidiurnal tides that average about 2.1 m with extremes of 3.2 m (station 9439026). Though the estuary supported extensive freshwater and brackish tidal wetlands including Sitka spruce swamp, much of these habitats have been diked for grazing and rural development and many of the small streams have been channelized (Lev et al. 2006). The upper portion of the watershed has been heavily harvested for timber, as well. The

Cooperage Slough site (CS02 and CS03; Figure 1B) supports soft-stem bulrush *Schoenoplectus tabernaemontani*), Nootka rose (Rosa nutkana), Douglas' spiraea (*Spiraea douglasii*), coastal willow (*Salix caroliniana*), and lady fern (*Athyrium filix-femina*). Lyngbye's sedge (*Carex lyngbyei*), lady fern (*Athyrium filix-femina*), soft-stem bulrush (*Schoenoplectus tabernaemontani*), coastal willow (*Salix caroliniana*), and Pacific water parsley (*Oenanthe sarmentosa*) are dominate species at the Daggett Point site (DP01, DP02, and DP03; Figure 1B). The Wallooskee Youngs (WY04; Figure 1B) site, which is low marsh and located outside a dike, primarily supports Lyngbye's sedge (*Carex lyngbyei*), soft-stem bulrush (*Schoenoplectus tabernaemontani*), and common spikerush (*Eleocharis palustris*; Brophy et al. 2017).

Tillamook Bay, which is 56 km^2, is the largest estuary and watershed in this study. Five rivers, the Miami, Kilchis, Wilson, Trask, and Tillamook, drain the 1,361-km^2 basin (Figure 1C; Komar et al. 2004). The area of Tillamook Bay tidal wetlands is estimated at 22.3 km^2 (Ewald and Brophy 2012). The mean tide range is 2.6 m and extreme tides can reach 3.7 m (station 9437540; NOAA). Diking that facilitates dairy farming dominates land alteration near the Bay, while much of the Coast Range has been logged for timber. Additionally, a series of wildfires known as the Tillamook burns occurred between 1931 and 1954 spanning 707 km^2 of forest within the Tillamook Bay watershed (Komar et al. 2004). The primary vegetation found at the Bay Marsh site (BM01 and BM02; Figure 1C) is creeping bentgrass (*Agrostis stolonifera*), Lyngbye's sedge (*Carex lyngbyei*), tufted hairgrass (*Deschampsia cespitosa*), reed canarygrass (*Phalaris arundinacea*), Pacific silverweed (*Potentilla pacifica*), and coastal willow, while the Dry Stocking Island site (DSI01 and DSI02; Figure 1C) is composed mostly of Lyngbye's sedge (*Carex lyngbyei*), Olyney's three-square bulrush (*Schoenoplectus americanus*), and tufted hairgrass

(*Deschampsia cespitosa*). The Goose Point site (GP01 and GP02; Figure 1C) exhibited tufted hairgrass (*Deschampsia cespitosa*), Pacific silverweed (*Potentilla pacifica*), Sitka spruce (*Picea sitchensis*), saltgrass (*Distichlis spicata*), and slough sedge (*Carex obnupta*; Brown et al. 2016).

The Salmon River Estuary, immediately south of Cascade Head, is the second smallest estuary in Oregon with a watershed of 194 km^2 and a 3.5-km^2 estuary (Figure 1D). Tidal wetlands in the Salmon River Estuary were estimated at 2.3 km^2 (Adamus et al. 2005). The mean, diurnal, and extreme tide ranges are 1.8, 2.5, and 5.2 m, respectively (U.S. Forest Service 1976). About 75% of the estuary was diked, primarily for agriculture, in the early 1960s (Frenkel and Morlan 1991). Most of the dikes have since been removed in accordance with restoration goals of Cascade Head Scenic Research Area and much of the estuary is tidal wetland. The high marsh site selected in the Salmon River Estuary (SR01, SR02, SR03, and SR04; Figure 1D) is dominated by Pacific silverweed (*Potentilla pacifica*), Baltic rush (*Juncus balticus*), and tufted hairgrass (*Deschampsia cespitosa*; Gray 2005).

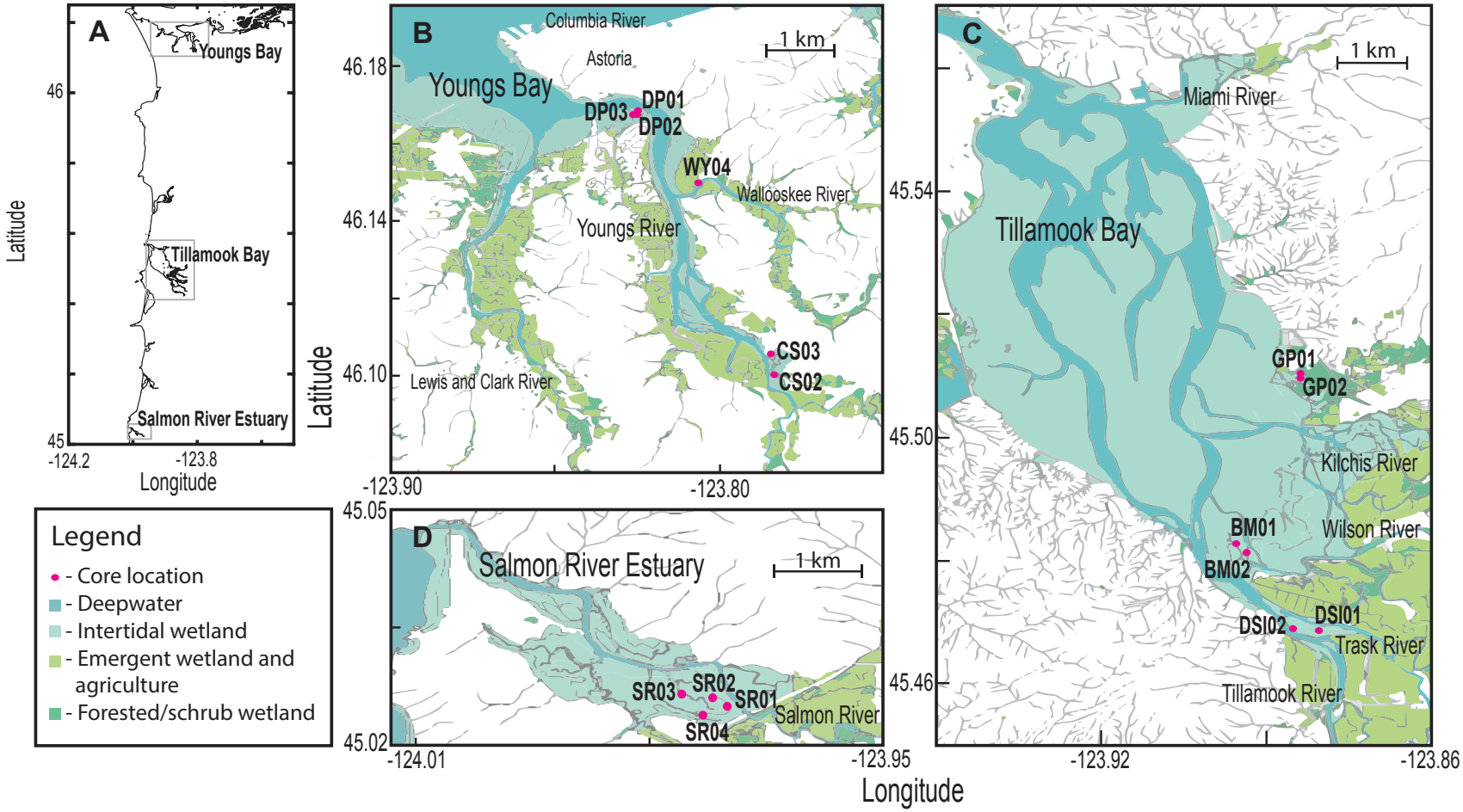

Figure 1. Maps depicting core locations within the intertidal wetlands of each estuary. Maps were created using the National Wetlands Inventory (U.S. Fish and Wildlife Service 2016). Subfigures A, B, C, and D show the northern portion of the Oregon coast, Youngs Bay, Tillamook Bay, and the Salmon River Estuary, respectively.

2.2 Estimating sea level change

Accurate determination of RSL change over the last century along the PNW coast is challenging. The Cascade margin, which extends from Vancouver Island in the north to Cape Mendocino, CA in the south, is a tectonically active subduction zone characterized by collision of the Juan de Fuca, Explorer, and Gorda plates with the North American plate. Along-margin interseismic uplift is variable, typically -1 to 4 mm yr^{-1} (Mazzotti et al. 2008), and combined with ESL rise causes differing rates of RSL change along the PNW coast. Moreover, elevation changes exhibit extreme eastward tilting from the coast, inland. Long-term trends of changing sea level are difficult to extract from short-term variations in climate due for example to El Niño/La Niña Southern Oscillation. The direction and speed of coastal winds and thus ocean surface currents vary seasonally along the PNW coast. Northerly winds push water off-shore during summer months upwelling cold, dense water; conversely, water pushed on-shore by southerly winds during winter months causes ocean surface temperatures to rise. Thus the region experiences winter sea levels higher than mean water elevation caused by convergence at the coast and thermal expansion (Komar et al. 2011). Additionally, the presence of a strong El Niño weakens upwelling, causing warmer sea surface temperatures and sea level rise. During particularly strong El Niños, such as 1982-83 and 1997-1998, mean sea level can rise as much as 30 cm (Komar 1998). Relative to the East and Gulf Coasts, the NOAA tide gauge record for Oregon is spatially and temporally limited, further complicating sea level change estimations.

Given this complexity, RSL rise in each of the three estuaries was calculated as regional ESL rise minus benchmark survey derived land-elevation changes. Benchmark uplift rates, provided in the Burgette et al. (2009) auxiliary material, were interpolated using natural neighbor

interpolation (Sibson 1981) for the Oregon coast (Figure 2); uplift rates at each core location were determined from this interpolation. Mean uplift rates for Youngs Bay, Tillamook Bay, and the Salmon River Estuary were 2.2 ± 0.1, 1.1 ± 0.1, and 1.1 ± 0.0 mm yr^{-1}, respectively (Table I), and are consistent with those published for the Astoria and South Beach NOAA tide gauges by Mazzotti et al. (2008).

Though others have employed a single value for ESL change along the entire PNW coast in calculating RSL change (e.g., Komar et al. 2011), regionally specific ESL changes were used here to produce moderately more refined rates. Mazzotti et al. (2008) calculated ESL rise rates by deriving precise RSL change rates and Global Positioning System (GPS)-derived vertical velocities for tide gauges along the PNW coast and then calculating regional 20^{th} century rates of ESL rise. These ESL changes were verified with 1993 – 2003 satellite altimetry. The Astoria tide gauge, located at the mouth of the Columbia River, is the closest gauge for the Youngs Bay sites and experiencing a ESL rise of 2.5 ± 1.1 mm yr^{-1}. Because the Tillamook Bay and Salmon River Estuary sites sit between the Astoria and South Beach gauges, a linear relationship of latitude and ESL change was used to estimate rates for these estuaries (ESL = -0.76 Lat – 38). Based on this interpolation, ESL is rising at rates of 3.0 ± 1.0 and 3.4 ± 0.9 mm yr^{-1} within Tillamook Bay and the Salmon River Estuary, respectively. These values combined with mean uplift rates yielded RSL rise rates of 0.28 ± 0.44, 1.8 ± 0.4, and 2.2 ± 0.3 mm yr^{-1} in Youngs Bay, Tillamook Bay, and the Salmon River Estuary, respectively (Table I).

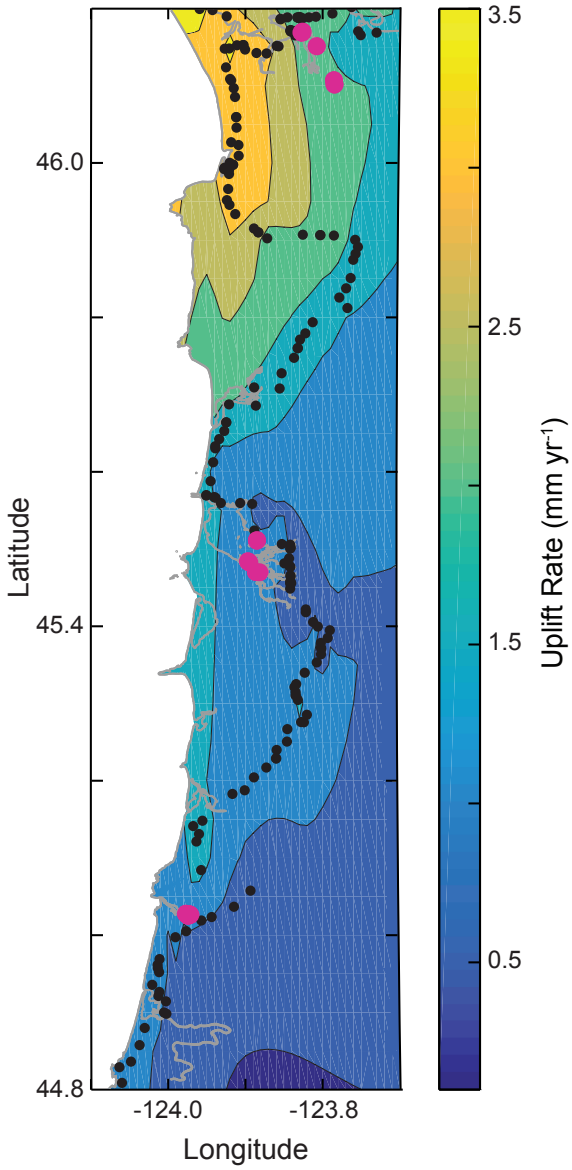

Figure 2. Distribution of uplift rates on the Oregon Coast interpolated using GPS velocities measured at benchmarks (black dots) along highways (Burgette et al. 2009). Pink dots represent coring locations.

Table I. Estimates of RSL, calculated using the average uplift rate for each estuary, and sediment loads for each estuary. The standard deviations of the uplift rates and ESL errors were used in calculating RSL error by standard error propagation laws (Taylor 1997). Loads were additionally estimated for Youngs Bay and the Salmon River Estuary based on the calculated value for Tillamook. Because these values are rough approximations, no error has been estimated. Watershed information, such as mean annual precipitation, mean basin elevation, relief, and geology are additionally presented.

Estuary	Uplift (mm yr^{-1})	ESL (mm yr^{-1})	RSL (mm yr^{-1})	Mean annual precipitation at USGS gauge [a] (cm)	Mean basin elevation [a] (m)	Relief [a] (m)	Geology [b]		Sediment load (x 10^3 t yr^{-1})	Load relative to Salmon River Estuary
							Igneous (%)	Sedimentary (%)		
Youngs Bay	2.2 ± 0.2	2.5 ± 1.1	0.28 ± 0.44	312	287	977	15	85	39	2x
Tillamook Bay	1.1 ± 0.1	3.0 ± 1.0	1.8 ± 0.4	318	507	1079	56	44	160	7x
Salmon River Estuary	1.1 ± 0.0	3.4 ± 0.9	2.2 ± 0.3	295	375	1033	53	47	24	x

[a](Risley et al. 2008); [b](Oregon Department of Geology and Mineral Industries 2015)

2.3 Estimating river sediment load

River sediment loads (t yr^{-1}) are typically estimated using discharge and suspended sediment concentration data, which is collected by the U.S. Geological Survey (USGS) (e.g., Syvitski et al. 2000; Wheatcroft and Sommerfield 2005). Unfortunately, many streams are ungauged within the PNW and the existing gauge records are often short, discontinuous, or incomplete. The Youngs River stream gauge (USGS 14251500) had daily discharge records from 1927 to 1958 but no record of sediment concentration. Similarly, a stream gauge along a small tributary of the Salmon River (Alder Brook; USGS 14303700) was a crest-stage partial record site (1954-1983) and therefore collected no continuous record of discharge. Both the Wilson and Trask Rivers within the Tillamook watershed are continuously monitored for daily discharge and sporadically measured for suspended sediment concentrations by the USGS. Though the Wilson River's records span 1931 – present (USGS 14301500), the Trask record only extends from 1961 to the present with a gap between 1971 and 1996 (USGS 14302480). Furthermore, the suspended sediment concentrations data were likely not representative of the stream conditions because sampling took place over limited time periods and multiple measurements were anomalous. The Kilchis and Tillamook Rivers are not gauged.

Fortunately however, sediment yield, which is the river's load normalized to its drainage area (t km^{-2} yr^{-1}), does not vary greatly amongst small, coastal rivers of the PNW (Karlin 1980). This is because Oregon watersheds, including the Youngs, Tillamook, and Salmon River, share similar characteristics such as geology, precipitation, and relief (Table I) that influence the magnitude of sediment delivered to the coastal ocean. Thus, we decided to determine a mean yield for the major rivers along the Oregon Coast based on available literature and apply this value in

calculating each basin's load. This assumption is reasonable given that the differences in magnitude of sediment loads between each estuary was most relevant to this study rather than absolute load estimates.

Published estimates of sediment yield from small mountainous rivers were tabulated for much of the Oregon Coast, from the Nehalem River in the north to the Coquille River in the south. Sediment yield averaged 120 ± 30 t km^2 yr^{-1}, with a range of 62 – 150 t km^2 yr^{-1} (Table II).

Table II. Published sediment yields for the tributaries of the major estuaries along the Oregon Coast. The periods of record are shown for values that were calculated from gauges, where P indicates present. Sediment yields that had been estimated from adjacent river basins are marked with an asterisk (*).

Coastal river	Sediment yield (t km^{-2} yr^{-1})	Period of record	Estimated from adjacent river basin	Source
Nehalem	125		*	Karlin 1980
Wilson, Trask, & Tillamook	125		*	Karlin 1980
Nestucca	125		*	Karlin 1980
Siletz	125		*	Karlin 1980
Yaquina	128.8	1973 - 1974		Karlin 1980
Alsea	75	1939 - P		Wheatcroft and Sommerfield 2005
Siuslaw	62	1967 - 1994		Wheatcroft and Sommerfield 2005
Umpqua	147	1905 - P		Wheatcroft and Sommerfield 2005
Coos	150		*	Wheatcroft and Sommerfield 2005
Coquille	150		*	Wheatcroft and Sommerfield 2005
Mean	**120 ± 30**			
Range	**62 - 150**			

Application of this yield to the 319 km^2 Youngs River watershed, 1290 km^2 Tillamook watershed, and 194 km^2 Salmon River watershed produced loads of 39 x 10^3, 160 x 10^3, and 24 x 10^3 t yr^{-1}, respectively (Table I). The Tillamook drainage area excluded the Miami River tributary as it is unlikely to contribute significate sediment to core locations. Due to the large differences in area between these basins, Youngs Bay and Tillamook Bay experience sediment loads approximately 2 and 7 times greater than observed in the Salmon River Estuary (Table I).

2.4 Field sampling

Sampling took place during 2015. Sediment cores were collected within the tidal wetlands in the elevation range of 1.68 to 2.89 m from Youngs Bay (n = 5) Tillamook Bay (n = 6), and the Salmon River Estuary (n = 4; Table III). Youngs Bay and Tillamook Bay cores were taken from low marsh, high marsh, and scrub-shrub tidal wetlands; in the Salmon River Estuary, cores were only collected in the high marsh. Coring locations were selected based on field reconnaissance and review of available data, including elevation, aerial photographs, vegetation, and sediment survey maps. PVC pipes that were 10-cm in diameter and either 1.5-m or 3-m in length, were first driven into the wetland using a sledge hammer. Elevations of sediment surface immediately surrounding the cores were made using a Real Time Kinematic (RTK) GPS (Table III). A truck jack attached via a pipe clamp was used to extract the cores. Both a stainless-steel core catcher riveted to the driving end of the core and a mechanical test plug inserted at the top of the sediment column helped prevent sediment loss during core retrieval. In the field, each long core was cut into two ~1.5 m sections using a pipe cutter. Cores were upright during transport back to the laboratory.

Table III. Data including coordinates and elevations for each core location within the three estuaries.

Site	Wetland type	Latitude	Longitude	Elevation (m)
Youngs Bay				
CS02	high marsh	46.100258	-123.783328	2.58
CS03	scrub-shrub	46.105755	-123.784042	2.69
DP01	low marsh	46.168694	-123.824684	1.81
DP02	high marsh	46.167595	-123.825140	2.89
DP03	scrub-shrub	46.167601	-123.826196	2.78
WY04	low marsh	46.149797	-123.806411	1.68
Tillamook Bay				
BM01	low marsh	45.482743	-123.895447	2.15
BM02	high marsh	45.481372	-123.893608	2.29
DSI01	high marsh	45.468665	-123.880499	2.61
DSI02	low marsh	45.468999	-123.885187	1.96
GP01	high marsh	45.509622	-123.883855	2.62
GP02	scrub- marsh	45.510250	-123.883781	2.74
Salmon River Estuary				
SR01	high marsh	45.025000	-123.969989	2.62
SR02	high marsh	45.026008	-123.971903	2.46
SR03	high marsh	45.026397	-123.975814	2.37
SR04	high marsh	45.023875	-123.973056	2.43

2.5 CT analysis

Soon after collection, all core sections were scanned at 0.5-mm resolution using a Toshiba Aquilion 64-slice Computed Tomography (CT) unit in Oregon State University's Veterinary Hospital. CT imaging provides non-destructive, high-resolution, 3D views of sediment stratigraphy that include physical and biogenic sedimentary structures (e.g., Davey et al. 2011). Because X-ray attenuation primarily varies with the gravimetric density of a material, CT imaging can also be used to quantify sediment bulk density. Denser materials attenuate X-rays more than less dense ones and result in lower grayscale values. We sought to determine a relationship

between CT-derived grayscale value and density to calculate sediment bulk densities within the core samples.

The CT scans were stored as image stacks in Digital Imaging and Communications in Medicine (DICOM) file format. Image stacks were processed using Fiji, a distribution of the open-source software ImageJ developed by the National Institutes of Health (Schneider et al. 2012). Following conversion to Tagged Image File Format (tiff), the stacked images were adjusted from a 12-bit Hounsfield unit (HU) range (-1024 to 3072) commonly used in medical imaging (Hendee and Ritenour 1992) to an 8-bit range (0 to 255) to complete other image processing procedures. Undecomposed large roots and rhizomes had to be removed from the stacked images as they do not contribute to sediment bulk density. A Fiji plugin, "Trainable Weka Segmentation", segmented the image into two classifications, sediment and live plant material based on standard training features (Arganda-Carreras et al. 2014). These segmentations were visually verified in each image stack. The live plant material field was subtracted from the original image stack and the mean grayscale value of the sediment was determined for each 1-mm image slice in the axial plane. These mean grayscale values were then averaged for each 2-cm vertical increment.

Others have derived a linear relationship between X-ray attenuation and density using calibration rods of known gravimetric density (e.g., Davey et al. 2011). However, X-ray attenuation additionally depends on the chemical composition of the scanned material with higher atomic numbers producing greater attenuation, and the calibration rods may fail to incorporate the influence of such sedimentary components. For instance, iron sulfides, which are often common in tidal wetlands, produce disproportionally high grayscale values causing an overestimation of sediment bulk density. Thus, gravimetric density of the sediment was analytically determined and

compared to the CT-derived grayscale values. After the cores had been split lengthwise, dry bulk density was measured by weighing a 0.5 or 1.0 cm^3 sediment sample extracted by a syringe every 2 cm for the top ~50 cm of each core before and after 24 h in a 60 °C drying oven. Salt in the pore water was not corrected for as it accounted for less than 1.9% of the wet weight or less than 3.2% of the dry weight. The measured dry bulk densities could then be compared with the corresponding mean grayscale values.

2.6 Sediment analysis

The other halves of the split cores were sampled at 2-cm increments and freeze dried. Large plant material was removed with forceps and the dried sediment was ground to a consistent texture using a mortar and pestle.

Samples were analyzed for percent OM by a standard loss-on-ignition (LOI) technique as recommended by Heiri et al. (2001): 1.000 ± 0.001 g of dried, disaggregated sediment was weighed into a crucible, burned at 550 °C for 4 h, and reweighed after cooling. LOI derived OM was correlated with C_{org} by measuring a subset of samples by elemental analysis (e.g., Craft et al. 1991; Goñi and Thomas 2000). The subset included at least two sediment samples from each core, one that had the highest organic content and one that was the lowest to ensure a representative curve.

Samples were prepared for γ-ray spectroscopy by placing on average 29 g of dried, disaggregated sediment in pre-weighed polystyrene counting jars. Samples were counted for ≥ 24 h on two essentially identical Canberra GL2020RS LEGe planar γ-ray spectrometers. ^{210}Pb and ^{214}Pb activities were measured at 46.5 and 351.9-keV photopeaks, respectively to calculate supported or excess ^{210}Pb ($^{210}Pb_{xS}$) activities and ^{137}Cs was measured using the 661.6 keV photopeak.

Sediment accumulation rates were calculated using the constant initial concentration (CIC) model (Sanchez-Cabeza and Ruiz-Fernández 2012, and the references therein). As the name implies, the CIC model assumes that the $^{210}Pb_{xS}$ activity of initially deposited material is constant over time. Although deposition can be somewhat variable, this assumption is valid on the timescales observed here (i.e., 100-150 yr). Assuming relatively constant sedimentation and negligible bioturbation, $^{210}Pb_{xS}$ is determined by a balance of advection and decay:

$$S\frac{\partial A}{\partial z} = -\lambda A \quad \text{(eq. 1).}$$

where S is the sediment accumulation rate (cm yr^{-1}), A is $^{210}Pb_{xS}$ activity (Bq kg^{-1}), λ is the ^{210}Pb decay constant (0.03101 yr^{-1}), and z is the depth (cm). At 0 cm depth, $A_z = A_0$ and A_z is 0 when z = ∞, the linear solution is:

$$A_z = A_0 e^{\left(\frac{-\lambda}{S}\right)z} \qquad \text{(eq. 2).}$$

The slope ($\frac{\lambda}{S}$) of a least squares line fit to A_z plotted with z yields a long-term average S (Wheatcroft et al. 2013; Cochran et al. 1998). Associated 95% confidence limits were calculated for the Ss using standard parametric statistics.

Although also delivered to the wetland surface via atmospheric fallout, ^{137}Cs is an anthropogenic radionuclide produced during nuclear fission and was first released into the environment during nuclear weapons testing around 1954. Input of ^{137}Cs reached a maximum preceding the Nuclear Test Ban Treaty in 1963. Within a sediment column, the first appearance and largest peak of ^{137}Cs are thus 1954 and 1963, respectively. Accounting for the depth of bioturbation, the depth of accumulated sediment since these time points provides an estimate of S (Ritchie and McHenry 1990).

3. Results

3.1 CT scans

CT images showed that the sediment cores were in good shape following extraction and transport as many biogenic and sedimentary structures typical of wetland sediment were well preserved within the top 50 cm of each core (Figure 3), and obvious artifacts of coring were not present. Often, the top 5 to 15 cm of sediment was darker than the rest of the core, indicating relatively low bulk density and high organic content (e.g., Figure 3 C, H, I, and J). This horizon is composed of recently accumulated OM that has not yet fully physically and biologically decomposed. Interestingly, some of the Youngs Bay cores had limited plant material (Figure 3 A – F) either indicating more recent colonization by marsh plants or greater decomposition of the vegetation. Roots and rhizomes were abundant throughout the top 50 cm of many cores (e.g., Figure 3 G – P). When concentrated towards the surface, these dense root mats may prevent bioturbation explaining the lack of obvious burrow holes, as others have noted (i.e., Richard 1978; McCaffery and Thomson 1980; Orson et al. 1998; Kolker et al. 2009). Some cores had layers of denser sediment indicating higher inorganic content (e.g., Figure 3 I – K). Because these layers had moderately sharp contacts with minimal post-depositional mixing and are present at similar depths within the three cores, they are suggestive of flood deposits. The Salmon River Estuary cores (particularly Figure 3 M, N, and P) exhibited many layers and thus little bioturbation.

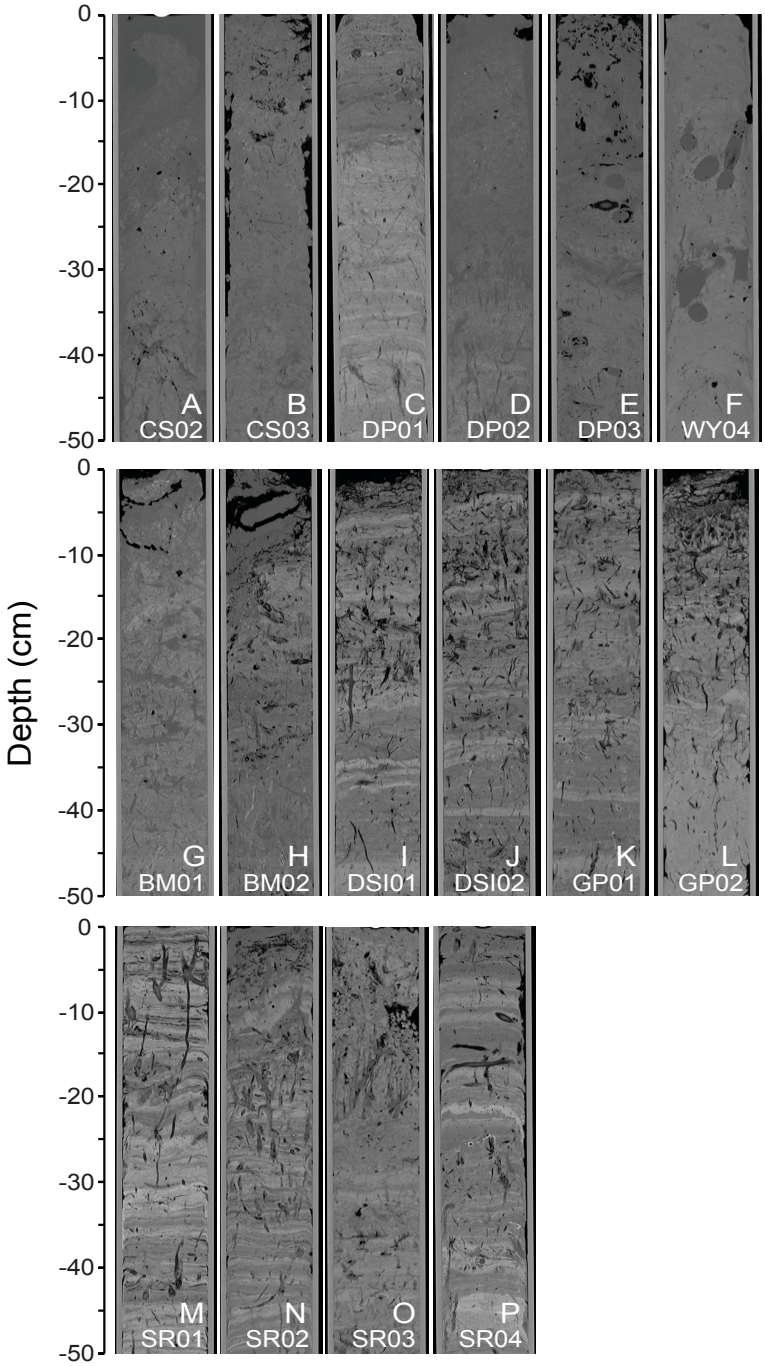

Figure 3. Top 50 cm of each CT scan. Lighter regions are more X-ray dense, while darker regions are less dense. Subplots A – F, G – L, and M – P were collected from Youngs Bay, Tillamook Bay, and the Salmon River Estuary, respectively.

3.2 Bulk density

Binned CT X-ray attenuation measured on an 8-bit grayscale (0-255) had a significant positive relationship with dry bulk density (Figure 4). This exponential regression was used to calculate dry bulk density from the CT scans when direct measurements had not been collected or were not valid, such as core DP02, which had desiccated during other laboratory procedures.

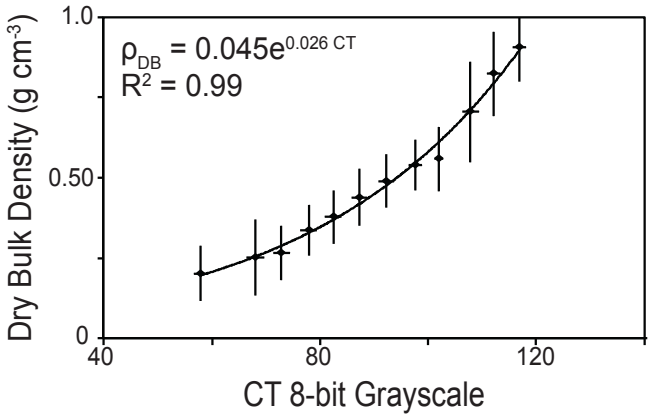

Figure 4. The relationship between dry bulk density (ρ_{DB}) measured gravimetrically every 2 cm for the top ~50 cm of each core and CT-derived 8-bit grayscale value (0-255) measured in the corresponding increments. Data (n = 301) were binned into five grayscale units (e.g., 55-60, 60-65, 65-70, etc.). The point from bin 60-65 was not included because only one datum fell within this range. The vertical and horizontal error bars represent the standard deviations of the average dry bulk density and CT grayscale value in each bin, respectively.

Density profiles within the top 50 cm of most cores showed a slight trend towards increasing with depth (Figure 5) due to greater decay of less-dense OM in older sediments and self-weight consolidation. Like the CT scans, little down-core variability was present within the Youngs Bay bulk density profiles apart from DP01 (Figure 5A). This core exhibited a lithologic change observable in the CT scan (Figure 3C). The density profiles of Tillamook (Figure 5B) and Salmon River (Figure 5C) generally show greater variability, which is unsurprising given their

complex stratigraphy. Comparison of the mean dry bulk density within the top 50 cm of each core to tidal elevation reveals a significant relationship (R^2 = 0.46; p-value = 0.004) in which bulk density increases at lower elevations. Low tidal elevations are inundated longer resulting in greater deposition of lithogenic material and reduced organic matter production.

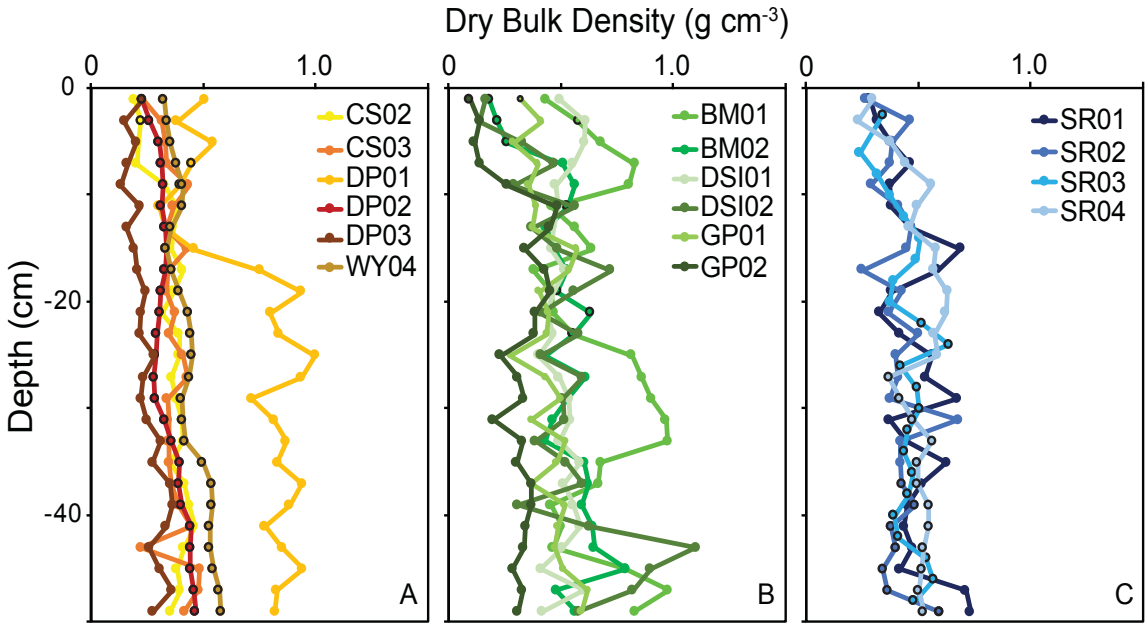

Figure 5. Density with depth measured within the top 50 cm of each core. Points without the black outline were measured analytically and points with the black outline were calculated using the CT scans and the relationship determined between dry bulk density and CT grayscale value (Figure 4). Sub-figures A, B, and C represent Youngs Bay, Tillamook Bay, and the Salmon River Estuary, respectively.

3.3 Organic matter and carbon contents

There was a strong relationship (R^2 = 0.99; n = 34) between LOI-derived OM and C_{org} measured by elemental analysis (Figure 6):

$$C_{org} = 0.29\ LOI + 0.0021\ LOI^2 \qquad \text{(eq. 3)}.$$

The conversion factor of 0.29 falls within the range of conversion factors calculated by others; for instance, 0.225 by Morris and Whiting (1986) and 0.40 by Craft et al. (1991). Given

the closeness of fit for all three estuaries, 0.29 is appropriate for least disturbed wetland sediments in northern Oregon. This relationship was applied to all core samples to convert OM to C_{org}. Interval C_{org} values ranged from as high as 40% in core GP02 to as low as 1.0% in core BM01.

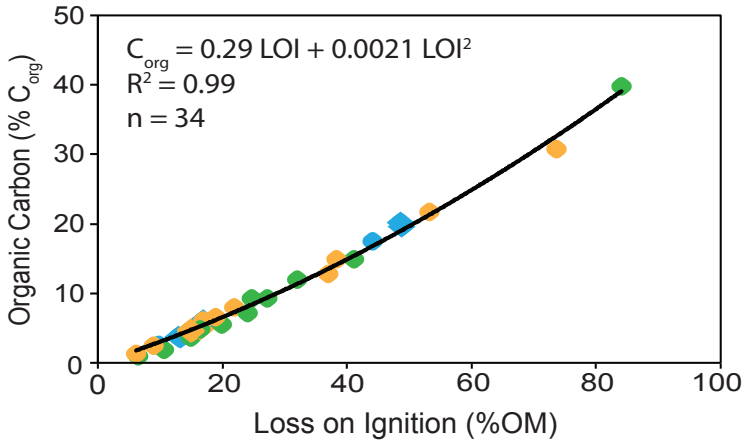

Figure 6. The relationship between OM as determined by LOI and OM measured by elemental analysis in a subset of samples from the three estuaries The subset included at least two sediment samples from each core, one that had the highest organic content and one that was the lowest to ensure a representative curve. Orange, green, and blue points refer to Youngs Bay, Tillamook Bay and the Salmon River Estuary, respectively.

The quadratic relationship between C_{org} and OM is explained by the relationship between C_{org} and nitrogen (N; Figure 7). Sediments that are enriched in OM are subject to greater remineralization by heterotrophic bacteria and detritivores, which require macro-nutrients such as N. As OM becomes enriched in high C_{org} content compounds (e.g., refractory organic compounds, fatty acids, and methane) through decomposition, the ratio of C_{org}:OM increases while the ratio of N: C_{org} decreases.

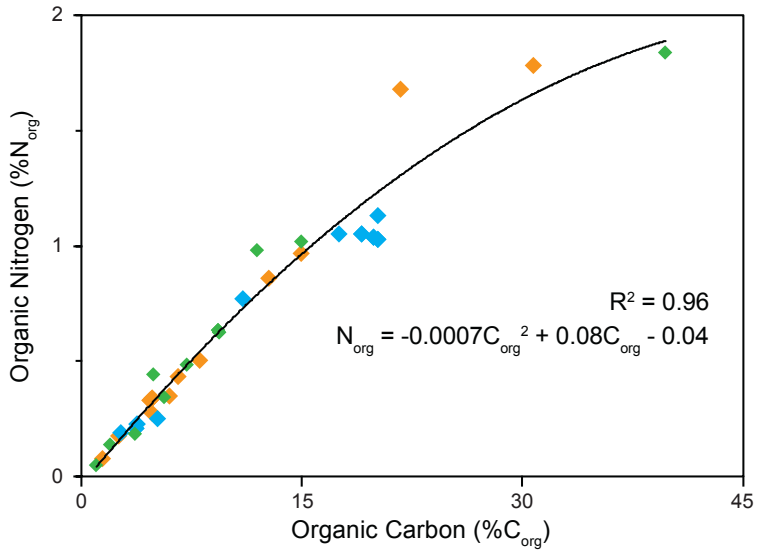

Figure 7. The relationship between C_{org} and N contents. Orange, green, and blue points refer to Youngs Bay, Tillamook Bay and the Salmon River Estuary, respectively.

Unsurprisingly most profiles of C_{org} content decline with depth (Figure 8) similar to density trends. Organic carbon in cores from Youngs Bay (Figure 8A; CS03 and WY04) and Tillamook Bay (Figure 8B; BM01 and DSI01) show no change within the top 50 cm, however. In the cases of WY04 and BM01, their low marsh position may hinder much autochthonous OM production.

Sediment carbon density ($\rho_{C_{org}}$; g cm^{-3}) was measured within the top 50 cm of each core as the product of dry bulk density and C_{org}. Unlike dry bulk density, mean sediment carbon density did not show a clear trend with elevation. Confounding variables, such as salinity, likely influence carbon density as well (Ouyang and Lee 2014).

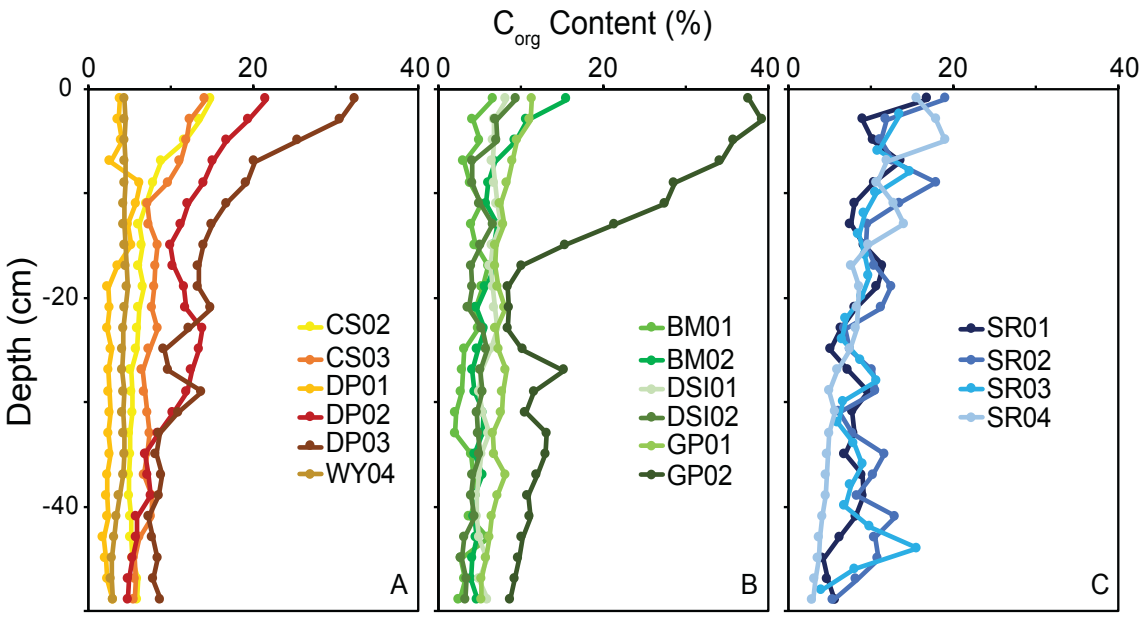

Figure 8. C_{org} content with depth for each core. Sub-figures A, B, and C represent Youngs Bay, Tillamook Bay, and Salmon River estuary, respectively.

3.4 Radiochronologies and accumulation rates

Surface activities of $^{210}Pb_{xS}$ ranged widely from 53 – 514 Bq kg^{-1} and penetration depths ranged from 16 – 90.5 cm (Figure 9, 10, and 11). Except for two cores, BM01 (Figure 10A) and DSI02 (Figure 10D), that displayed nonsteady state accumulation, profiles of $^{210}Pb_{xS}$ activity with depth approximated an idealized profile (MacKenzie et al. 2011) and were readily interpretable (Figure 9, 10, and 11). Guidelines were developed to determine which intervals should be included in the regression to calculate Ss. Intervals with counting errors ranging below the detection limit of the γ-ray spectrometers (3 Bq kg^{-1}) were excluded. Though $^{210}Pb_{xS}$ profiles presented within the literature often show clear indication of a surface mixing layer in which activities in the top 10 cm are constant before exponentially decaying (e.g., Wheatcroft and Sommerfield 2005), none of the $^{210}Pb_{xS}$ profiles suggest significant bioturbation. The presence of dense root mats common to tidal

wetlands may have prevented much mixing; as stated above, the CT images lack many obvious burrows and often exhibit complex root and rhizome matrixes (e.g., Figure 3 G – P). Three cores had surface sediment organic contents that diluted the lithogenic component causing low $^{210}Pb_{xS}$ activities (GP01, DP01, and DP03); these data were omitted, as well. Multiple profiles exhibit outliers due either to a change in lithology or possible non-local bioturbation, which were additionally excluded from the regression equation (e.g., SR03, BM02, DSI01, and DP02). Less than 25% of the data points were excluded from the regressions.

The mean accretion rates for the high marsh and scrub-shrub wetland sites in Youngs Bay, Tillamook Bay, and the Salmon River Estuary were 2.7 ± 0.6, 2.2 ± 0.3, and 2.4 ± 0.7 mm yr^{-1}, respectively. There is no evidence that these means are different (one-way ANOVA, $p = 0.5$) and thus the mean S for all three estuaries is 2.4 ± 0.5 mm yr^{-1} ($n = 12$).

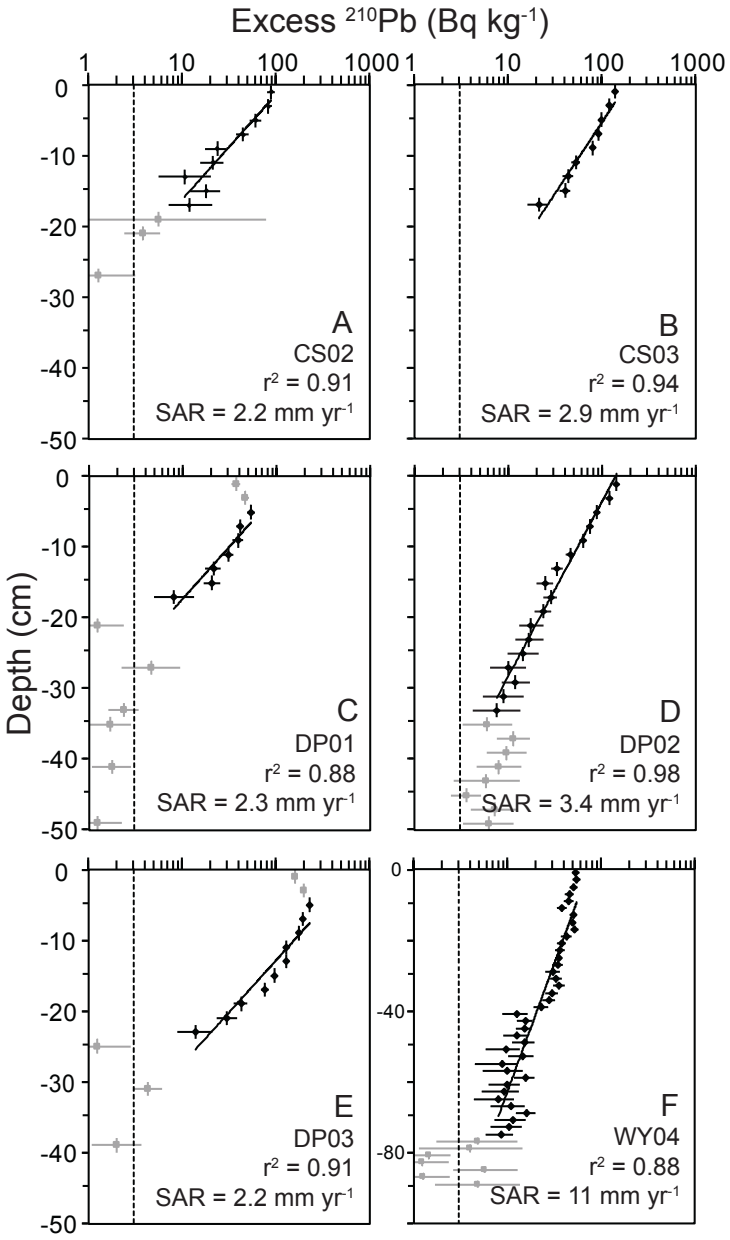

Figure 9. Profiles of $^{210}Pb_{xS}$ activities with depth in Youngs Bay cores measured by γ-ray spectroscopy. Note that the x-axis is logarithmic. Fits were used in calculating Ss by the CIC model. Horizontal error bars represent counting errors calculated specifically for each γ counter, while vertical error bars represent the 2-cm-thick sampling interval. Grey data points are those not included in the exponential fit. The vertical dotted line at 3 Bq kg^{-1} represents the detection limit. Note that the depth axis scale has changed for WY04 (Subfigure F).

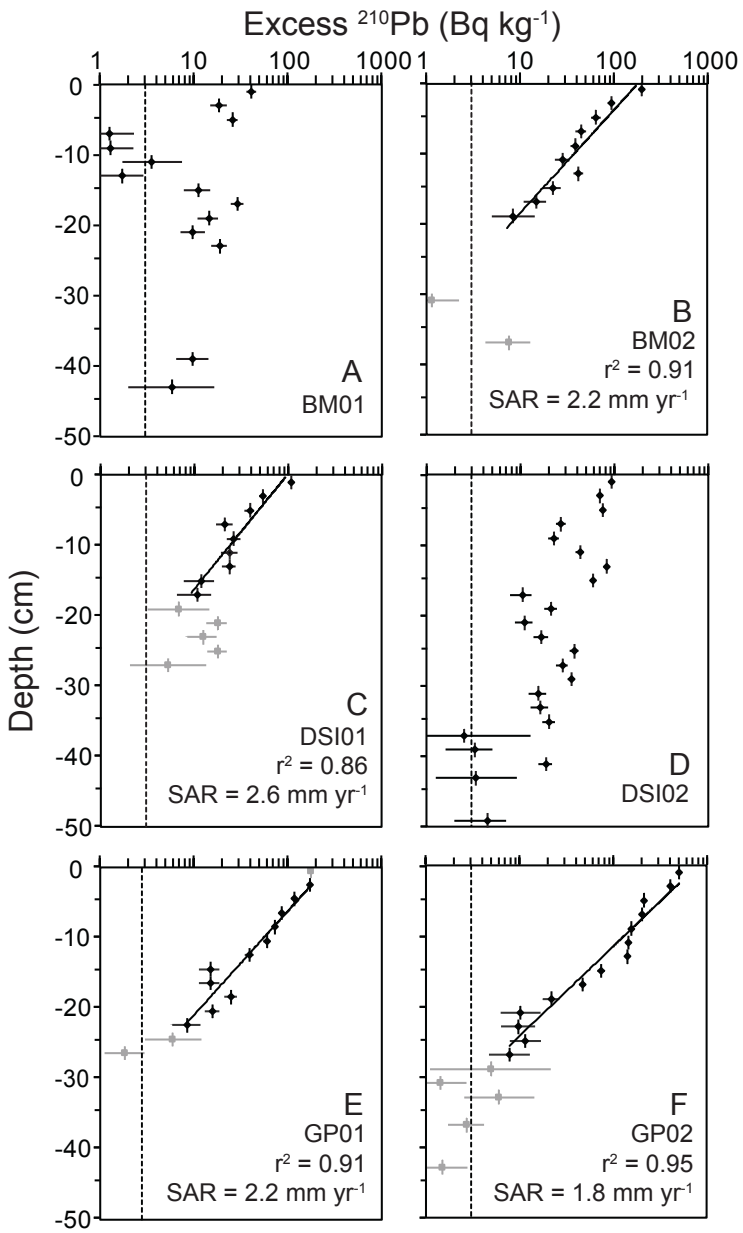

Figure 10. Profiles of $^{210}Pb_{xS}$ activities with depth in Tillamook Bay cores measured by γ-ray spectroscopy. See Figure 9 for details.

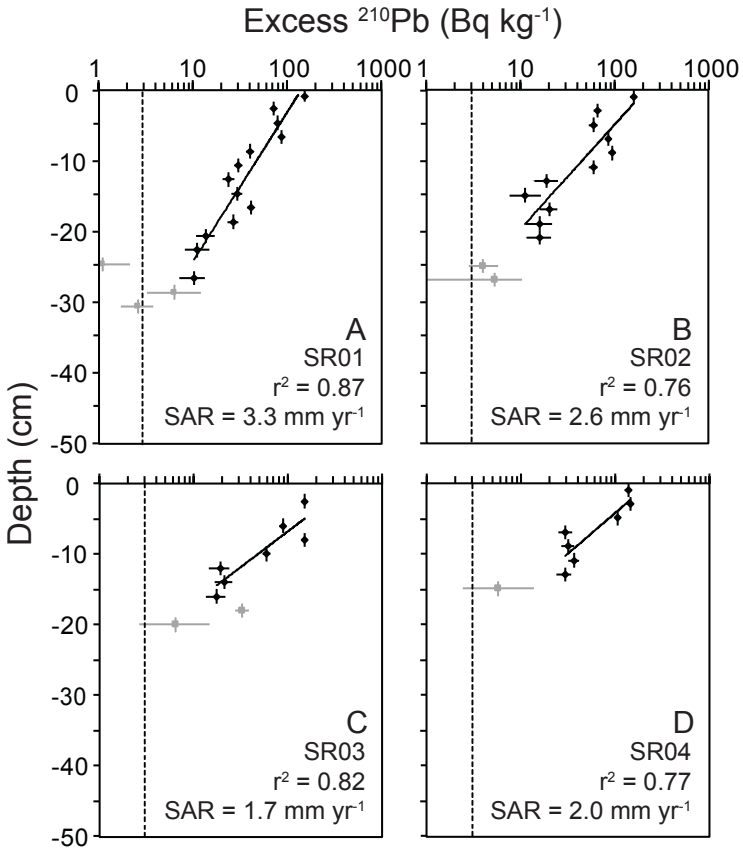

Figure 11. Profiles of $^{210}Pb_{xS}$ activities with depth in Salmon River Estuary core measured by γ-ray spectroscopy. See Figure 9 for details.

Many of the cores either had no ^{137}Cs activities above the detection limit or exhibited anomalous ^{137}Cs profiles indicative of post depositional remobilization (Foster et al. 2006), in which the activity peaked at or near the sediment surface and was much higher (40 - 320 Bq kg^{-1}) than expected given unaltered sorption. However, the cores that displayed exceptionally fast sediment accumulation (>10 mm yr^{-1}) had preserved ^{137}Cs profiles (e.g., BM01, DSI02, WY04; Figure 12). Because the ^{210}Pb profiles of BM01 and DSI02 show nonsteady state deposition, the ^{137}Cs calculated Ss have been used. The WY04 core however showed good agreement between dating methods and thus these independently calculated Ss were averaged.

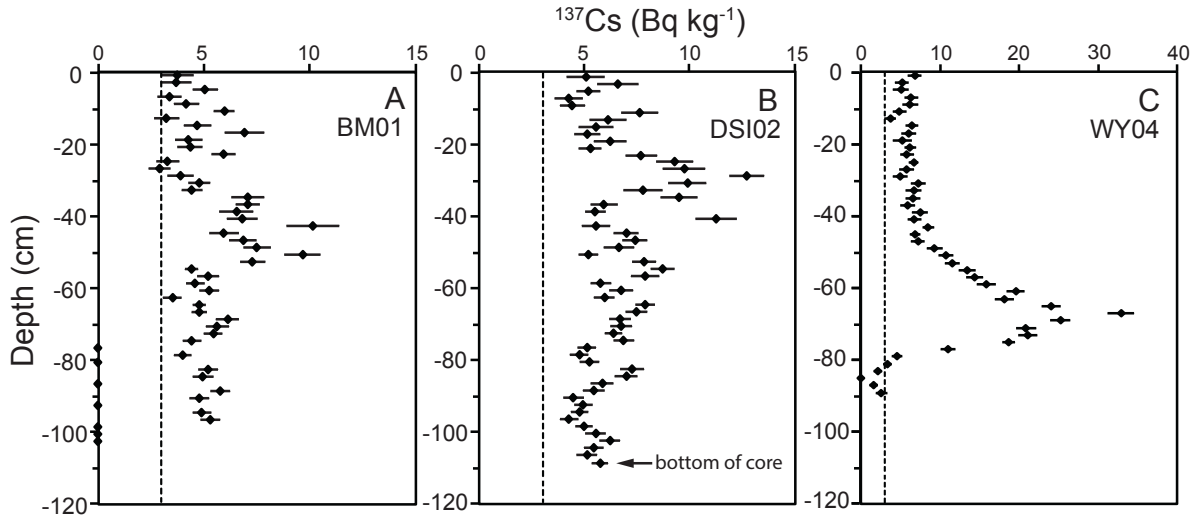

Figure 12. Profiles of ^{137}Cs activities with depth in low marsh cores measured by γ-ray spectroscopy. Horizontal error bars represent errors calculated specifically for each γ counter, while vertical error bars represent the 2-cm-thick sampling interval. The vertical dotted line at 3 Bq kg^{-1} represents the detection limit.

Three cores collected within low marsh, WY04, BM01, and DSI02, exhibited high Ss, 12 ± 1, 10 ± 3, and >18 mm yr^{-1} respectively. Historical aerial photographs reveal that these tidal wetlands have been expanding horizontally (Brophy pers comm. 2016). These rapidly accreting, low marsh sites were not included in mean estimates of Ss. The Daggett Point site DP01 was additionally excluded in mean high marsh accretion rate calculations since it was collected in low marsh though it did not exhibit rapid accretion.

Mass accumulation rate (MAR; g m^{-2} yr^{-1}) was calculated from the slope ($\frac{\lambda}{\mathrm{MAR}}$) of a least squares line fit to A_z plotted against the cumulative mass (g cm^{-2}; Sanchez-Cabeza and Ruiz-Fernández 2012). Even though there were minimal changes in dry bulk density as a function of depth (Figure 5), MARs are often preferred measures of accumulation as they better account for sediment compaction than Ss. Again, there was no evidence that the mean MARs are different

(one-way ANOVA, $p = 0.7$). The average MAR for all three estuaries is 0.94 ± 0.31 kg m^{-2} yr^{-1} (Table IV).

Carbon mass accumulation rates (CARs; g C_{org} m^{-2} yr^{-1}) were calculated as the product of S and carbon density averaged over the accumulation rate depth (Callaway et al. 2012). Low marsh cores (i.e., DP01, WY04, BM01, and DSI02) were additionally excluded from calculation of the mean CARs in each estuary. Youngs Bay, Tillamook Bay, and the Salmon River Estuary exhibited on average 87 ± 35, 85 ± 19, and 110 ± 30 g C_{org} m^{-2} yr^{-1}, respectively; these means are not statistically different (one-way ANOVA, $p = 0.4$). The average CAR for all three estuaries is 94 ± 33 g C_{org} m^{-2} yr^{-1} (Table IV)

Lastly, mineral deposition rate (MDR; g m^{-2} yr^{-1}) was calculated as the product of S and the average mineral density averaged over the accumulation rate depth (Callaway et al. 2012). Mineral densities were calculated as the product of dry bulk density and lithogenic fraction (i.e., 1-LOI) of each 2-cm increment. The average MDRs are not different between estuaries (one-way ANOVA, $p = 0.7$); the mean for all locations is 670 ± 250 g m^{-2} yr^{-1} (Table IV), excluding low marsh cores.

Table IV. Ss, C_{org} densities, MARs, CARs, and MDRs for each core from the three estuaries. Note that the low marsh values marked with an asterisk '*' are not included in the estuarine means, which are bolded.

Site	RSL (mm yr^{-1})	S (mm yr^{-1}) ^{210}Pb	S (mm yr^{-1}) ^{137}Cs	C_{org} Density (g cm^{-3})	MAR (kg m^{-2} yr^{-1})	CAR (g m^{-2} yr^{-1})	MDR (g m^{-2} yr^{-1})
Youngs Bay							
CS02	0.28 ± 0.44	2.2 ± 0.3		0.023 ± 0.003	0.71 ± 0.10	54 ± 7	550 ± 90
CS03		2.9 ± 0.3		0.029 ± 0.006	1.1 ± 0.1	100 ± 10	780 ± 70
DP01		2.3 ± 0.4 *		0.021 ± 0.004	0.93 ± 0.10 *	45 ± 6 *	790 ± 90 *
DP02		3.4 ± 0.1		0.035 ± 0.009	1.1 ± 0.0	130 ± 0	710 ± 30
DP03		2.2 ± 0.2		0.031 ± 0.011	0.42 ± 0.04	64 ± 7	250 ± 20
WY04		11 ± 1 *	13 ± 0	0.018 ± 0.002	6.1 ± 0.6 *	210 ± 10 *	4900 ± 1000 *
Mean		**2.7 ± 0.6**		**0.026 ± 0.007**	**0.83 ± 0.33**	**87 ± 35**	**570 ± 240**
Tillamook Bay							
BM01	1.8 ± 0.4		10 ± 3	0.025 ± 0.004	6.4 ± 1.7 *	260 ± 70 *	6600 ± 2700 *
BM02		2.2 ± 0.2		0.028 ± 0.005	1.0 ± 0.1	69 ± 8	830 ± 110
DSI01		2.6 ± 0.4		0.031 ± 0.005	1.3 ± 0.2	90 ± 13	1000 ± 140
DSI02			> 18	0.023 ± 0.006	> 7.9 *	> 420 *	> 12000 *
GP01		2.2 ± 0.2		0.033 ± 0.005	0.95 ± 0.10	72 ± 7	740 ± 80
GP02		1.8 ± 0.1		0.046 ± 0.024	0.63 ± 0.04	110 ± 10	370 ± 20
Mean		**2.2 ± 0.3**		**0.031 ± 0.008**	**0.97 ± 0.27**	**85 ± 19**	**740 ± 270**
Salmon River Estuary							
SR01	2.2 ± 0.3	3.3 ± 0.4		0.040 ± 0.013	1.5 ± 0.2	140 ± 20	1100 ± 100
SR02		2.6 ± 0.5		0.042 ± 0.008	1.0 ± 0.2	120 ± 20	670 ± 100
SR03		1.7 ± 0.4		0.040 ± 0.012	0.62 ± 0.12	63 ± 13	440 ± 90
SR04		2.0 ± 0.5		0.039 ± 0.018	0.92 ± 0.24	120 ± 30	590 ± 160
Mean		**2.4 ± 0.7**		**0.040 ± 0.002**	**1.0 ± 0.4**	**110 ± 30**	**700 ± 280**
Overall Mean		**2.4 ± 0.5**		**0.034 ± 0.007**	**0.94 ± 0.31**	**94 ± 33**	**670 ± 250**

4. Discussion

4.1 QA/QC retrospective

As previously stated, determining RSL change and sediment supply rates for the PNW is challenging and requires a fair bit of assumption and interpolation. For instance, both uplift and ESL rise rates were interpolated for each estuary necessitating the assumption that the available point measurements were representative. Rates of ESL rise have been corroborated with independent satellite measurements (1993 – 2003; Mazzotti et al. 2008), but unfortunately uplift rates and therefore RSL have not been verified. Additionally, calculation of the relative sediment loads for each estuary assumed they had similar watershed sediment yields. Though precipitation and relief are quite similar between systems, Tillamook Bay has a higher mean basin elevation indicating a larger potential for sediment erosion (Table I), whereas Youngs Bay has a much higher ratio of sedimentary to igneous lithology compared to the other watersheds. This difference in lithology could mean that the yield of the Youngs Bay watershed is higher. Despite the difficulties associated with calculating sediment load, the vast difference in watershed size supports the general trend of Tillamook having the largest sediment supply and the Salmon River having the smallest.

Suspended sediment concentration, rather than fluvial sediment load, may however have been a more apt comparison to sea level rise in studying tidal wetland accretion (e.g., Kirwan et al. 2016; Morris et al. 2016). Though sediment load likely effects suspended sediment concentration to a great degree, several other influences include input of marine sediment, distance from a tidal channel, tidal range, tidal velocity, wind wave intensity, and proximity to the estuarine turbidity maximum (Friedrichs and Perry 2001). Only sediment supply was considered because

the estuaries studied herein have a paucity of suspended sediment concentration data, and most influencing variables were assumed similar apart from load. This assumption should be validated by future studies. Additionally, mean annual values of sediment load may be a misleading representation of sediment supplied to estuaries due to the extreme episodic nature of PNW discharge. For instance on an annual scale, coastal rivers in the PNW discharge 80 to 95% of their water and sediment during winter storms (Karlin 1980). Interannual variability, particularly associated with El Niño/La Niña Southern Oscillation, causes shifts in annual precipitation and thus alters erosion and sediment transport. On a longer time scale, major floods, such as in 1972, 1964, 1996, and 2007, drastically increase sediment to the coastal ocean (Kniskern et al. 2011). Humans have additionally influenced fluvial sediment dynamics. From 1931 to 1954, a series of wildfires associated with logging burned 707 km^2 of forest in the Tillamook basin, enhancing sediment supply by 29% (Komar 2004). Damming in the PNW may limit sediment flux to periods of high water (Karlin 1980) and decrease sediment output; as evidence, damming on the Columbia River has primarily caused the estimated 60% decrease in sediment flux (Borde et al. 2003). Clearly, an average annual sediment load may be too simplistic, so perhaps the episodic nature of sediment supply could be linked by future studies to patterns of sediment deposition and accumulation using more immediate measurements of elevation change. For instance, sedimentation-erosion tables (SETs) provide both event-based measurements and long-term trends of sediment accretion (Boumans and Day 1993).

In determining mean accumulation rates representative of an estuary's tidal wetlands, heterogeneity within the wetland environment necessitates comprehensive sampling. Though only 16 cores were collected between the three estuaries, there is good agreement in accumulation rates

for each estuary's high marsh and scrub-shrub tidal wetland locations. A Grubbs test for statistical outliers revealed no outliers ($\alpha = 0.05$) amongst high elevation cores.

In most cores, excepting WY04, we have used only one age dating technique – $^{210}Pb_{xS}$ or ^{137}Cs. When sedimentation is rapid, such as 10 ± 3 and >18 mm yr^{-1} observed in BM01 and DSI02, ^{137}Cs appears more resistant to remobilization caused by changes in pore water redox chemistry (Figure 12), but $^{210}Pb_{xS}$ profiles do not permit estimates of sediment accumulation (Figure 10 A and D). Slower, steadier rates of accumulation (i.e. 1.7 – 3.4 mm yr^{-1}) result in less changes in lithology and $^{210}Pb_{xS}$ profiles that logarithmically decrease with depth, but allow post-depositional remobilization of ^{137}Cs. Although multiple authors have suggested ^{210}Pb may be mobilized due to redox processes during early diagenesis or due to aerobic degradation of OM (Allen et al. 1993), ^{210}Pb is less mobile than ^{137}Cs within tidal wetland environments due to its complexation with sulfur to form PbS (Crusius and Anderson 1991). Though there has been remobilization of ^{137}Cs it is unlikely that this is the case for ^{210}Pb. The validity of the method combined with the readily interpretable radionuclide profiles add considerable weight to our calculated rates of accumulation, and the derived rates (i.e., MAR, CAR, and MDR).

4.2 Sediment accretion rates

Comparison of the two estuaries with the greatest difference in sediment load – Tillamook Bay and the Salmon River Estuary – can best determine whether RSL change or sediment supply primarily controls the formation and growth of tidal wetlands. Tillamook Bay and the Salmon River Estuary differ by a factor of greater than 7 in sediment load; however, 20^{th} century RSL rise has been statistically similar in these regions, 1.8 ± 0.4 and 2.2 ± 0.3 mm yr^{-1} respectively. The mean Ss within these two estuaries, 2.2 ± 0.3 mm yr^{-1} in Tillamook Bay and 2.4 ± 0.7 mm yr^{-1} in

the Salmon River Estuary, are not only also statistically similar (one-way ANOVA, $p = 0.6$), but vary with the slight difference in RSL rise. This pattern suggests that increased hydroperiods and accommodation space created under RSL rise principally controls vertical accretion within northern Oregon tidal wetlands.

Youngs Bay, which has an approximately stable sea level (0.28 ± 0.44 mm yr^{-1}), currently accretes at a mean rate of 2.7 ± 0.6 mm yr^{-1}, which is about 9 times faster than the estimated RSL rise. Though not statistically significant, this mean S is larger than that observed in Tillamook which has a 4-fold greater sediment load. This suggests our initial assumptions about Youngs Bay RSL and sediment supply may be incorrect.

Underestimation of the relative rate of sea level rise within Youngs Bay is a possibility. The record of ESL change in this region of the PNW coast is primarily based on the nearby Astoria gauge. Enhanced elevation of local sea level by the Columbia River outflow may invalidate use of the 0.30 ± 0.22 mm yr^{-1} rate of ESL rise (Mitchell et al. 1994). Moreover, the interpolated uplift rates rely on a small number of benchmarks, and the sites in which CS02 and CS03 were collected are 8.5 km from the closest benchmarks (Figure 2). Alternatively, we may have not accurately estimated the relative sediment supply to the Youngs Bay system. The large ratio of sedimentary to igneous rocks in the watershed may lead to greater sediment yield. Youngs Bay may additionally be experiencing increased sediment supply from the Columbia River system. However, it is unlikely that either RSL rise within Youngs Bay is 2.3 mm yr^{-1} higher or that sediment supply is greater than in Tillamook Bay. As previously stated, our consideration of sediment load rather than suspended sediment concentration may be the culprit. Youngs Bay may in fact have a higher mean

suspended sediment concentration than Tillamook Bay, causing the elevated Ss. Similar, future studies should focus on less complicated systems.

4.3 PNW tidal wetlands resilience

The average S for each estuary is greater than each region's estimated RSL rise. However, both Tillamook Bay and Salmon River Estuary exhibit cores (i.e., 1.8 ± 0.1 mm yr^{-1} at GP02, and 1.7 ± 0.4 mm yr^{-1} at SR03) with sediment accretions lower than their associated sea level rise (1.8 ± 0.4 and 2.2 ± 0.3 mm yr^{-1}, respectively), though consideration of the accompanying error indicates overlap in values (Table IV). Interestingly, the reasons for these deviations seem to be very different. In the case of the Tillamook core, GP02 sits at the highest elevation, meaning it experiences the shortest hydroperiod and thus the shortest timeframe during which sediment can accumulate. It is possible that as sea level continues to rise, this location will begin accreting faster. Moreover, though this site has the lowest S, its CAR is greater than the other Tillamook Bay cores at steady state with RSL. Wetland habitats that sit high in the tidal frame experience less mineral loading than those lower in elevation, and thus organic accretion is often greater (Morris et al. 2016).

Conversely, SR03 sits at the lowest elevation amongst the Salmon River coring locations. SR03 is the closest to a large channel and thus may be slightly erosional. To investigate this possibility, inventories of $^{210}Pb_{xS}$ (Q, Bq cm^{-2}) were calculated as:

$$Q = \sum_{i} (\rho_i h_i A_i) \qquad \text{(eq. 4)}$$

where ρ_i is the dry bulk density, h_i is the thickness of the interval, and A_i is the activity at the *i*th depth interval (Cochran et al. 1998). The Salmon River cores had an average inventory of 0.41 ± 0.07 Bq cm^{-2}, yet SR03 had the lowest inventory of 0.35 ± 0.03 Bq cm^{-2}. Minor erosion of up to

33% may therefore be possible. Alternatively, larger grain size within the sediment core, possibly given its location near the channel, would reduce the $^{210}Pb_{xS}$ inventory; however, the dry bulk density profiles (Figure 5C) show no striking differences between the lithologies of the Salmon River cores.

The three cores with exceptionally high Ss (BM01, DSI02, and WY04) are all located within low marsh. The capacity for low elevation regions of Oregon tidal wetlands to accrete 5 times greater than high marsh areas highlights the potential for these environments to persist under accelerated RSL rise. Kirwan et al. (2016) note that vertical accretion within lower elevations may be the best indication of tidal wetland resilience under future rates of sea level rise. This is because high marsh regions vertically accrete to a high elevation within the tidal frame, thereby reducing frequent flooding, but low marsh regions are often inundated, simulating the stress of accelerated RSL. If these areas continue accreting under such stress, the tidal wetland may avoid future drowning. The low marsh Youngs Bay core, DP01 had a S of 2.3 ± 0.4 mm yr^{-1}; though this site is not accreting as rapidly as the other low marsh core collected in Youngs Bay (WY04), it is still 8 times faster than the estimated RSL rise in this region.

Kirwan et al. (2010) showed that the maximum rate of sea level rise a wetland is capable of withstanding is strongly limited by the amount of available sediment. In fact, most examples of drowned tidal wetlands involve sediment starvation (e.g., Mississippi River Delta, Chesapeake Bay, and Venice Lagoon; Weston 2014). Rough calculations of mass accumulated over the wetland surfaces each year compared to estimated annual sediment loads indicate no dearth of available allochthonous material. The area of Tillamook Bay tidal wetlands is estimated at 22.3 km^2 (Ewald and Brophy 2012). Considering an average mass accumulation over this entire area of

930 g m^{-2} yr^{-1}, about 21 x 10^3 t of sediment are deposited on tidal wetlands each year. With an estimated sediment load of 160 x 10^3 t yr^{-1}, most sediment is exported to the shelf each year. Tidal wetlands in the Salmon River estuary, which has the greatest tidal wetland area relative to estuarine area in Oregon, were estimated at 2.3 km^2 (Adamus et al. 2005). The MAR of 980 g m^{-2} yr^{-1} results in 2.5 x 10^3 t of sediment deposited on the wetland annually. The estimated sediment load for the Salmon River Estuary is 39 x 10^3 t yr^{-1}, so that most fluvial sediment, 36 x 10^3 t yr^{-1}, is also exported to the shelf. All else being equal, it does not appear that wetland accretion in Oregon estuaries will be sediment limited. This is in stark contrast to estuaries along the U.S. East and Gulf Coasts (Weston 2014).

Rates of ESL rise projected by the National Research Council (NRC; 2012) in Newport, OR are summarized in Table V. The projected rate is the mean value presented by Pardaens et al. (2011) and the worst-case scenario value was calculated from the range provided by the IPCC (2007). Assuming these values are representative of the northern portions of the coast and assuming coastal uplift rates remain constant, RSL rise rates were calculated for the three estuaries, as well. Current RSL rise calculated for Youngs Bay is the same as the NRC's projected value of 0.30 mm yr^{-1}, but Tillamook Bay's current RSL rise rate is more similar to the worst-case scenario value for 2000 to 2030. If Tillamook Bay and the Salmon River Estuary maintain steady state with RSL rise, mean Ss within these tidal wetlands will likely reflect the NRC's projected rates of RSL increase. Additionally, because CARs tend to reflect Ss (Chmura et al. 2003), CARs may also increase proportionally to rates of RSL rise. Thus, if the worst-case sea level rise scenario proves correct, carbon burial may increase by 500 and 410% for Tillamook Bay and the Salmon River

estuary, respectively. Limits to autochthonous carbon production will assuredly dampen CARs, though (Morris et al. 2016).

Table V. NRC's (2012) projected and worst-case scenario rates of ESL rise for the next century. RSL rise rates were calculated assuming ESL values are similar for more northern portions of the OR coast and assuming uplift rates remain constant in the three estuaries.

	ESL (mm yr^{-1})	RSL (mm yr^{-1})		
		Youngs Bay	Tillamook Bay	Salmon River Estuary
2000 – 2030				
Projected	2.5	0.30	1.4	1.4
Worst-case	3.2	1.0	2.1	2.1
2030 – 2050				
Projected	4.6	2.4	3.5	3.5
Worst-case	6.4	4.2	5.3	5.3
2050 – 2100				
Projected	7.6	5.4	6.5	6.5
Worst-case	10.6	8.4	9.5	9.5

4.4 Global C_{org} cycle context

Accurate estimates of carbon burial within tidal wetlands are not only important for local management and for incentivizing habitat protection, accurate global sequestration rates are additionally vital to creating a comprehensive understanding of the global carbon cycle and its influence on climate. Many of the planet's coastlines are understudied, but few of the U.S. tidal wetlands are as understudied as the Oregon Coast. In fact, San Francisco, CA and Puget Sound, WA often represent all West Coast estuaries; however, these are inapt comparisons as 95% of Californian coastal wetlands have been converted for other land-use (Morris et al. 2012), while Puget Sound is a partially urbanized fjord having lost 70% of its wetlands (Emmett et al. 2000).

Mean sediment carbon density measured within these sites averaged 0.032 ± 0.008 g cm^{-3}, similar to the global mean of 0.039 ± 0.003 g cm^{-3} for tidal wetlands (Chmura et al. 2003). However, the mean carbon burial rate for the three estuaries, 94 ± 33 g C_{org} m^{-2} yr^{-1}, is less than

half the global burial flux of 245 ± 26 g C_{org} m^{-2} yr^{-1} and roughly two times less than the 173 ± 45 g C_{org} m^{-2} yr^{-1} calculated for the northeast Pacific region based on California data (Ouyang and Lee 2014). Chmura et al. (2003) found that sediment accretion rates were the primary contributing factor to carbon burial, and so the relatively low rates of CAR observed in these tidal wetlands can be attributed to low Ss due to below average mean RSL rise rates. Establishing vertical accretion rates and whether Oregon tidal wetlands are in steady state with RSL rise is therefore vital in predicting carbon burial potential.

Though the CARs for Tillamook Bay and the Salmon River Estuary are statistically similar (one-way ANOVA, $p = 0.1$), the mean value for the Salmon River Estuary is slightly greater (Table IV). C_{org} accretion may thus be slightly affected by the available sediment load, but because the dominant factor affecting the CAR is the S (Chmura et al. 2003), which is a function of RSL, no strong correlation is expected. Interestingly, Youngs Bay, which had the fastest S had a statistically similar mean CAR (one-way ANOVA, $p = 0.4$). Additionally, though its RSL rise was the slowest, the mean MDR was statistically similar to the mean MDRs in Tillamook Bay and the Salmon River Estuary (one-way ANOVA, $p = 0.7$). This is not surprising given the similar mean Ss measured in the three estuaries; however, it means that even when out of steady state with RSL rise, CAR and MDR are still primarily impacted by S. The slightly smaller values may be due to rapid accretion that has not yet allowed for significant compaction.

5. Conclusions and future work

- Despite a sevenfold difference in sediment loads, Tillamook Bay and the Salmon River Estuary exhibit similar sediment accumulation rates that approximate RSL rise rates within each estuary. Therefore, RSL rise appears to control vertical accretion. This conclusion is further

supported when considering that sediment accretion rates reflect RSL rise in Tillamook Bay despite the dramatic increase in sediment supply during the mid-century wildfires.

- Though experiencing 0.28 ± 0.44 mm yr^{-1} RSL rise, Youngs Bay high marshes are accreting at 2.7 ± 0.6 mm yr^{-1}. It appears that either we have miscalculated sea level rise within this region, or an additional source of sediment has heightened accretion in Youngs Bay tidal wetlands.
- Rapid accretion measured within several low elevation cores and export of excess suspended sediment from the estuaries suggest Oregon wetlands will be resilient in the face of future accelerated RSL rise rates.
- Vertical accretion and thus RSL rise appears to additionally control C_{org} burial rates as evidenced by similar mean CARs in Tillamook Bay and the Salmon River Estuary. Because RSL rise along the Oregon coast is less than global rates and the areal extent of these tidal wetlands is small, the PNW likely does not sequester C_{org} at a globally significant magnitude.

Future work will expand the methods utilized here to four other Oregon estuaries – Nehalem, Alsea, Umpqua, and Coquille – to further assess the competing effects of RSL rise and sediment supply on vertical accretion. Continuation of this work may better elucidate reasons for the apparently high rates of sediment accretion in Youngs Bay. Additionally, comparisons to sediment erosion table (SET) data (Boumans and Day 1993) may allow us to determine the importance of episodic events on sediment accretion in the PNW. As ideal natural laboratories, Oregon estuaries could be used to better understand the concept of alternate stable states in influencing tidal wetland morphology, as well.

Citations

Adams, W.A. 1973. The effect of organic matter on the bulk and true densities of some uncultivated podzolic soils. *Journal of Sediment Science 24*: 10-17.

Adamus, P.R., J. Larsen, and R. Scranton. 2005. Wetland profiles of Oregon's coastal watersheds and estuaries: Part 3 of a hydrogeomorphic guidebook. Report to Coos Watershed Association. U.S. Environmental Protection Agency and Oregon Department of State Lands, Salem, OR.

Allen, J.R., J.E. Rae, G. Longworth, S.E. Hasler, and M. Ivanovich. 1993. A comparison of the ^{210}Pb dating technique with three other independent dating methods in an oxic estuarine salt-marsh sequence. *Estuaries and Coasts 16*: 670-677.

Appleby, P.G., and F. Oldfield. 1978. The calculation of lead-210 dates assuming a constant rate of supply of unsupported ^{210}Pb to the sediment. *Catena 5*: 1-8.

Arganda-Carreras, I., V. Kaynig, J. Schindelin, A. Cardona, and H.S. Seung. 2014. Trainable weka segmentation: a machine learning tool for microscopy image segmentation. <http://www.sfn.org/~/media/SfN/Documents/Short Courses/2014 SC 2/SC 2 Chapters/Ignacio ArgandaCarreras.ashx>.

Balistrieri, L.S., J.W. Murray, and B. Paul. 1995. The geochemical cycling of stable Pb, ^{210}Pb, and ^{210}Po in seasonally anoxic Lake Sammamish, Washington, USA. *Geochimica et Cosmochimica acta 59*: 4845-4861.

Barbier, E.B., S.D. Hacker, C. Kennedy, E.W. Koch, A.C. Stier, and B.R. Silliman. 2011. The value of estuarine and coastal ecosystem services. *Ecological Monographs 81*: 169-193.

Barnes, R.S., P.B. Birch, D.E. Spyridakis, and W.R. Schell. 1979. Changes in the sedimentation histories of lakes using Lead-210 as a tracer of sinking particulate matter. *Isotope Hydrology 2*: 875 - 897.

Baskaran, M. 2011. Po-210 and Pb-210 as atmospheric tracers and global atmospheric Pb-210 fallout: a review. *Journal of Environmental Radioactivity 102*: 500-513.

Beck, M. W., K.L. Heck Jr, K.W. Able, D.L. Childers, D.B. Eggleston, B.M Gillanders, B. Halpern, C.G. Hays, K. Hoshino, T.J. Minello and R.J. Orth. 2001. The identification, conservation, and management of estuarine and marine nurseries for fish and invertebrates. *Bioscience 51*: 633-641.

Bellucci, L.G., M. Frignani, J.K. Cochran, S. Albertazzi, L. Zaggia, G. Cecconi, and H. Hopkins. 2007. ^{210}Pb and ^{137}Cs as chronometers for salt marsh accretion in the Venice Lagoon–links to flooding frequency and climate change. *Journal of Environmental Radioactivity 97*: 85-102.

Binford, M.W. 1990. Calculation and uncertainty analysis of ^{210}Pb dates for PIRLA project lake sediment cores. *Journal of Paleolimnology 3*: 253-267.

Boumans, R.M., and J.W. Day. 1993. High precision measurements of sediment elevation in shallow coastal areas using a sedimentation-erosion table. *Estuaries and Coasts 16*: 375-380.

Brophy, L.S. 2016. Interview by E.K. Peck [in person]. Blue carbon analysis at Wallooskee-Youngs (Youngs Bay, OR) and Southern Flow Corridor (Tillamook Bay, OR) restoration sites. Institute for Applied Ecology. Corvallis, OR.

Brophy, L.S., L.A. Brown, M.J. Ewald, and E.K. Peck. 2017. Baseline monitoring at Wallooskee-Youngs restoration site, 2015: Part 2. Corvallis, Oregon: Institute for Applied Ecology.

Brown, C.A. and R.J. Ozretich. 2009. Coupling between the coastal ocean and Yaquina Bay, Oregon: Importance of oceanic inputs relative to other nitrogen sources. *Estuaries and Coasts 32*: 219-237.

Brown, L.A., M.J. Ewald, L.S. Brophy, and S. van de Wetering. 2016. Southern Flow Corridor baseline effectiveness monitoring: 2014. Corvallis, Oregon: Estuary Technical Group, Institute for Applied Ecology. Prepared for Tillamook County, Oregon.

Borde, A.B., R.M. Thom, S. Rumrill, and L.M. Miller. 2003. Geospatial habitat change analysis in Pacific Northwest coastal estuaries. *Estuaries 26*: 1104-1116.

Boumans, R.M., and J.W. Day. 1993. High precision measurements of sediment elevation in shallow coastal areas using a sedimentation-erosion table. *Estuaries and Coasts 16*: 375-380.

Burgette, R.J., R.J. Weldon, and D.A. Schmidt. 2009. Interseismic uplift rates for western Oregon and along-strike variation in locking on the Cascadia subduction zone. *Journal of Geophysical Research: Solid Earth 114*: B01408.

Callaway, J.C., E.L. Borgnis, R.E. Turner, and C.S. Milan. 2012. Carbon sequestration and sediment accretion in San Francisco Bay tidal wetlands. *Estuaries and Coasts 35*: 1163-1181.

Chmura, G.L., S.C. Anisfeld, D.R. Cahoon, and J.C. Lynch. 2003. Global carbon sequestration in tidal, saline wetland soils. *Global Biogeochemical Cycles 17*: 1-22.

Cochran, J.K., M. Frignani, M. Salamanca, L.G. Bellucci, and S. Guerzoni. 1998. Lead-210 as a tracer of atmospheric input of heavy metals in the northern Venice Lagoon. *Marine Chemistry 62*: 15-29.

Cohn, T.A. 1995. Recent advances in statistical methods for the estimation of sediment and nutrient transport in rivers. *Reviews of Geophysics 33*: 1117-1123.

Colman, S.M., and J.F. Bratton. 2003. Anthropogenically induced changes in sediment and biogenic silica fluxes in Chesapeake Bay. *Geology 31*: 71-74.

Craft, C., J. Clough, J. Ehman, S. Joye, R. Park, S. Pennings, G. Hongyu, and M. Machmuller. 2009. Forecasting the effects of accelerated sea-level rise on tidal marsh ecosystem services. *Frontiers in Ecology and the Environment 7*: 73-78.

Craft, C.B., E.D. Seneca, and S.W. Broome. 1991. Loss on ignition and Kjeldahl digestion for estimating organic carbon and total nitrogen in estuarine marsh soils: calibration with dry combustion. *Estuaries and Coasts 14*: 175-179.

Crosby, S.C., D.F. Sax, M.E. Palmer, H.S. Booth, L.A. Deegan, M.D. Bertness, and H.M. Leslie. 2016. Salt marsh persistence is threatened by predicted sea-level rise. *Estuarine, Coastal and Shelf Science 181*: 93-99.

Crooks, S., J. Rybczyk, K. O'Connell, D.L. Devier, K. Poppe, S. Emmett-Mattox. 2014. Coastal blue carbon opportunity assessment for the Snohomish Estuary: The climate benefits of estuary restoration. Report by Environmental Science Associates, Western Washington University, EarthCorps, and Restore America's Estuaries.

Crusius, J., and R.F. Anderson. 1991. Immobility of ^{210}Pb in Black Sea sediments. *Geochimica et Cosmochimica Acta 55*: 327-333.

Dahl, T.E., and S.M. Stedman. 2013. Status and trends of wetlands in the coastal watersheds of the Conterminous United States 2004 to 2009. U.S. Department of the Interior, Fish and Wildlife Service, US National Oceanic and Atmospheric Administration, and National Marine Fisheries Service.

Davey, E., C. Wigand, R. Johnson, K. Sundberg, J. Morris, and C.T. Roman. 2011. Use of computed tomography imaging for quantifying coarse roots, rhizomes, peat, and particle densities in marsh soils. *Ecological Applications 21*: 2156-2171.

Day, J.W., L.D. Britsch, S.R. Hawes, G.P. Shaffer, D.J. Reed, and D. Cahoon. 2000. Pattern and process of land loss in the Mississippi Delta: a spatial and temporal analysis of wetland habitat change. *Estuaries and Coasts 23*: 425-438.

Emmett, R., R. Llansó, J. Newton, R. Thom, M. Hornberger, C. Morgan, C. Levings, A. Copping, and P. Fishman. 2000. Geographic signatures of North American west coast estuaries. *Estuaries 23*: 765-792.

Ewald, M.J., and L.S. Brophy. 2012. Tidal Wetland Prioritization for the Tillamook Bay Estuary. Prepared for the Tillamook Estuaries Partnership, Garibaldi, Oregon. Green Point Consulting, Corvallis, Oregon.

Foster, I.D., T.M. Mighall, H. Proffitt, D.E. Walling, and P.N. Owens. 2006. Post-depositional ^{137}Cs mobility in the sediments of three shallow coastal lagoons, SW England. *Journal of Paleolimnology 35*: 881-895.

French, J. 2006. Tidal marsh sedimentation and resilience to environmental change: exploratory modelling of tidal, sea-level and sediment supply forcing in predominantly allochthonous systems. *Marine Geology 235*: 119-136.

Frenkel, R.E., and J.C. Morlan. 1991. Can we restore our salt marshes? Lessons from the Salmon River, Oregon. *Northwest Environmental Journal. 7*: 119-135.

Friedrichs, C.T., and J.E. Perry. 2001. Tidal salt marsh morphodynamics: a synthesis. *Journal of Coastal Research 27*: 7-37.

Gedan, K.B., B.R. Silliman, and M.D. Bertness. 2009. Centuries of human-driven change in salt marsh ecosystems. *Annual Review of Marine Science 1*: 117-141.

Goñi, M.A., and K.A. Thomas. 2000. Sources and transformations of organic matter in surface soils and sediments from a tidal estuary (North Inlet, South Carolina, USA). *Estuaries 23*: 548-564.

Gonnea, M.E. 2016. Evaluation of the continuous rate of supply lead-210 sediment age model: Two sources of potential bias and implications for carbon burial rates (Abstract No. B11G-04). Paper presented at the meeting of the American Geophysical Union, San Francisco, CA.

Gray, A. 2005. The Salmon River estuary: restoring tidal inundation and tracking ecosystem response. Doctoral dissertation, University of Washington (Accession No. 3178142).

Heiri, O., A.F. Lotter, and G. Lemcke. 2001. Loss on ignition as a method for estimating organic and carbonate content in sediments: reproducibility and comparability of results. *Journal of Paleolimnology 25*: 101-110.

Hendee, W.R., and E.R. Ritenour. 1992. *Medical Imaging Physics*. Year Book Medical Pub.

Hickey, B.M., and N.S. Banas. 2003. Oceanography of the U.S. Pacific Northwest coastal ocean and estuaries with application to coastal ecology. *Estuaries and Coasts 26*: 1010-1031.

IPCC. 2007. Climate Change 2007: The Physical Science Basis. Contribution of Working Group I to the Fourth Assessment Report of the Intergovernmental Panel on Climate Change. Solomon, S., D. Qin, M. Manning, Z. Chen, M. Marquis, K.B. Averyt, M.Tignor and H.L. Miller, eds. Cambridge University Press, Cambridge, United Kingdom and New York, NY, USA.

Karlin, R. 1980. Sediment sources and clay mineral distributions off the Oregon coast. *Journal of Sedimentary Research 50*: 543-560.

Kirwan, M.L., and J.P. Megonigal. 2013. Tidal wetland stability in the face of human impacts and sea-level rise. *Nature 504*: 53-60.

Kirwan, M.L., G.R. Guntenspergen, A. D'Alpaos, J.T. Morris, S.M. Mudd, and S. Temmerman. 2010. Limits on the adaptability of coastal marshes to rising sea level. *Geophysical Research Letters 37*: L23401.

Kirwan, M.L., A.B. Murray, J.P. Donnelly, and D.R. Corbett. 2011. Rapid wetland expansion during European settlement and its implication for marsh survival under modern sediment delivery rates. *Geology 39*: 507-510.

Kirwan, M.L., S. Temmerman, E.E. Skeehan, G.R. Guntenspergen, and S. Fagherazzi. 2016. Overestimation of marsh vulnerability to sea level rise. *Nature Climate Change 6*: 253-260.

Kniskern, T.A., J.A. Warrick, K.L. Farnsworth, R.A. Wheatcroft, and M.A. Goñi. 2011. Coherence of river and ocean conditions along the US West Coast during storms. *Continental Shelf Research 31*: 789-805.

Kolker, A.S., S.L. Goodbred, S. Hameed, and J.K. Cochran. 2009. High-resolution records of the response of coastal wetland systems to long-term and short-term sea-level variability. *Estuarine, Coastal and Shelf Science 84*: 493-508.

Komar, P.D. 1998. The 1997-98 El Niño and erosion on the Oregon coast. *Shore and Beach 66*: 33-41.

Komar, P.D., J. McManus, and M. Styllas. 2004. Sediment accumulation in Tillamook Bay, Oregon: natural processes versus human impacts. *The Journal of Geology 112*: 455-469.

Komar, P.D., J.C. Allan, and P. Ruggiero. 2011. Sea level variations along the U.S. Pacific Northwest coast: Tectonic and climate controls. *Journal of Coastal Research 27*: 808-823.

Lev, E., D. Vander Schaaf, J. Christy, J. Anderson, P. Adamus, and K. Popper. 2006. Youngs Bay bottomlands conservation and restoration plan. The Wetlands Conservancy and The Nature Conservancy.

MacKenzie, A.B., S.M.L. Hardie, J.G. Farmer, L.J. Eades, and I.D. Pulford. 2011. Analytical and sampling constraints in ^{210}Pb dating. *Science of the Total Environment 409*: 1298-1304.

Mazzotti, S., C. Jones, and R.E. Thomson. 2008. Relative and absolute sea level rise in western Canada and northwestern United States from a combined tide gauge-GPS analysis. *Journal of Geophysical Research: Oceans 113*: C11019.

McCaffrey, R.J., and J. Thomson. 1980. A record of the accumulation of sediment and trace metals in a Connecticut salt marsh. *Advances in Geophysics 22*: 165-236.

Mitchell, C.E., P. Vincent, R.J. Weldon, and M.A. Richards. 1994. Present-day vertical deformation of the Cascadia Margin, Pacific Northwest, United States. *Journal of Geophysical Research: Solid Earth 99*: 12257-12277.

Morris, J.T., and G.J. Whiting. 1986. Emission of gaseous carbon dioxide from salt-marsh sediments and its relation to other carbon losses. *Estuaries and Coasts 9*: 9-19.

Morris, J.T., J. Edwards, S. Crooks, and E. Reyes. 2012. Assessment of carbon sequestration potential in coastal wetlands. In *Recarbonization of the Biosphere,* Lal, R., K. Lorenz, R.F. Huttl, B.W. Schneider, and J. von Braun, eds., Springer Netherlands. 517-531.

Morris, J.T., D.C. Barber, J.C. Callaway, R. Chambers, S.C. Hagen, C.S. Hopkinson, B.J. Johnson, P. Megonigal, S.C. Neubauer, T. Troxler, and C. Wigand. 2016. Contributions of organic and inorganic matter to sediment volume and accretion in tidal wetlands at steady state. *Earth's Future 4*: 110-121.

Mudd, S.M. 2011. The life and death of salt marshes in response to anthropogenic disturbance of sediment supply. *Geology 39*: 511-512.

National Research Council, 2012: Sea-level rise for the coasts of California, Oregon, and Washington: past, present, and future. The National Academies Press, Washington, DC.

Nevissi, A.E. 1985. Measurement of ^{210}Pb atmospheric flux in the Pacific Northwest. *Health Physics 48*: 169-174.

U.S. National Oceanic and Atmospheric Administration (NOAA). NOAA Tides and Currents: Datums. <https://tidesandcurrents.noaa.gov/stations.html?type=Datums>.

Oregon Department of Geology and Mineral Industries. 2015. Oregon Geologic Data Compilation (OGDC) – Release 6. <http://www.oregongeology.org/pubs/dds/ogdc/OGDC-6_report.pdf>

Orson, R.A., R.S. Warren, and W.A. Niering. 1998. Interpreting sea level rise and rates of vertical marsh accretion in a southern New England tidal salt marsh. *Estuarine, Coastal and Shelf Science 47*: 419-429.

Ouyang, X., and S.Y. Lee. 2014. Updated estimates of carbon accumulation rates in coastal marsh sediments. *Biogeosciences 11*: 5057-5071.

Pardaens, A.K., J.M. Gregory, and J.A. Lowe. 2011. A model study of factors influencing projected changes in regional sea level over the twenty-first century. *Climate Dynamics 36*: 2015-2033.

Richard, G.A. 1978. Seasonal and environmental variations in sediment accretion in a Long Island salt marsh. *Estuaries 1*: 29-35.

Risley, J., A.J. Stonewall, and T. Haluska. 2008. Estimating Flow-Duration and Low-Flow Frequency Statistics for Unregulated Streams in Oregon. U.S. Geological Survey Investigations Report 2008-5126: 0-22.

Ritchie, J.C., and J.R. McHenry. 1990. Application of radioactive fallout cesium-137 for measuring soil erosion and sediment accumulation rates and patterns: a review. *Journal of Environmental Quality 19*: 215-233.

Sanchez-Cabeza, J.A., I. Ani-Ragolta, and P. Masque. 2000. Some considerations of the ^{210}Pb constant rate of supply (CRS) dating model. *Limnology and Oceanography 45*: 990-995.

Sanchez-Cabeza, J.A., and A.C. Ruiz-Fernández. 2012. ^{210}Pb sediment radiochronology: an integrated formulation and classification of dating models. *Geochimica et Cosmochimica Acta 82*: 183-200.

Schneider, C.A., W.S. Rasband, and K.W. Eliceiri. 2012. NIH Image to ImageJ: 25 years of image analysis. *Nature Methods 9*: 671-675.

Sibson, R. 1981. A brief description of natural neighbor interpolation. *Interpreting Multivariate Data 21*: 21-36.

Syvitski, J.P., M.D. Morehead, D.B. Bahr, and T. Mulder. 2000. Estimating fluvial sediment transport: the rating parameters. *Water Resources Research 36*: 2747-2760.

Taylor, J.R. 1997. *An introduction to error analysis: the study of uncertainties in physical measurements.* 2nd ed. Sausalito, Calif.: University Science Books.

Thom, R.M. 1992. Accretion rates of low intertidal salt marshes in the Pacific Northwest. *Wetlands 12*: 147-156.

Thom, R.M., and A.B. Borde. 1998. Human intervention in Pacific Northwest coastal ecosystems. *Change in Pacific Northwest Coastal Ecosystems. GR McMurray and RJ Bailey, editors. NOAA Coastal Ocean Program, Decision Analysis Series*: 5-37.

Torio, D.D., and G.L. Chmura. 2013. Assessing coastal squeeze of tidal wetlands. *Journal of Coastal Research 29*: 1049-1061.

Turner, A., and G.E. Millward. 2002. Suspended particles: their role in estuarine biogeochemical cycles. *Estuarine, Coastal and Shelf Science 55*: 857-883.

U.S. Fish and Wildlife Service. 2016. National Wetlands Inventory website. U.S. Department of the Interior, Fish and Wildlife Service, Washington, D.C. < http://www.fws.gov/wetlands/ >.

U.S. Forest Service. 1976. Siuslaw National Forest (N.F.), Cascade Head Scenic Research Area management plan: Environmental impact statement. U.S. Forest Service, Washington, D.C. < https://www.fs.usda.gov/Internet/FSE_DOCUMENTS/fsbdev7_007114.pdf >.

U.S. Geological Survey (USGS). USGS Water Data for the Nation. < https://waterdata.usgs.gov/nwis >.

Weston, N.B. 2014. Declining sediments and rising seas: an unfortunate convergence for tidal wetlands. *Estuaries and Coasts 37*: 1-23.

Wheatcroft, R.A., and C.K. Sommerfield. 2005. River sediment flux and shelf sediment accumulation rates on the Pacific Northwest margin. *Continental Shelf Research 25*: 311-332.

Wheatcroft, R.A., M.A. Goñi, K.N. Richardson, and J.C. Borgeld. 2013. Natural and human impacts on centennial sediment accumulation patterns on the Umpqua River margin, Oregon. *Marine Geology 339*: 44-56.

Wissmar, R.C., and C.A. Simenstad. 1998. Variability of riverine and estuarine ecosystem productivity for supporting Pacific Salmon. Change in Pacific Northwest Coastal Ecosystems. GR McMurray and RJ Bailey, editors. NOAA Coastal Ocean Program, Decision Analysis Series: 253-301.

APPENDICES

Appendix I. Estimating sediment loads using Wilson River data

Though the suspended sediment concentration data collected at the Wilson River gauge (USGS 14301500) was primarily measured over a limited number of days within less than three consecutive years (November 2011 – February 2014), it is analyzed here for comparison to our previous load estimations.

To create rating curves for the Wilson River, values of suspended sediment concentration (C_t in g m^{-3}) were plotted against the instantaneous measurements of discharge (Q_t in m^3 s^{-1}) and a regression equation in the form of:

$$\ln C_t = \beta_0 + \beta_1 \ln Q_t + \varepsilon \qquad \text{(eq. 5)}$$

was fit to the data (Cohn et al. 1995; Figure 13). β_0 and β_1 are model coefficients and ε is the residual error. Suspended sediment concentration data were not included if the associated daily discharge was below the long-term average, as C_t values during low flow are significantly influenced by stream diatoms and other authigenic organic material in suspension (Wheatcroft and Sommerfield 2005). Bedload was not included though it may account for 10 to 20% of the total river load (Karlin 1980). Data were further culled to remove flagged values and obvious outliers, then averaged for days with multiple measurements. The power law relationships could then be applied to the long-term records of discharge measured at the same gauge stations to calculate daily records of suspended sediment concentration by:

$$C_t = e^{\left(\beta_0 + \beta_1 \ln Q_t + \frac{s^2}{2}\right)} \quad \text{(eq. 6)}$$

where s is the standard error of the residuals. River sediment loads (t yr^{-1}) are the product of suspended sediment concentration and daily discharge summed over a year, and lastly sediment yield is the river's load normalized to its drainage area (t km^{-2} yr^{-1}).

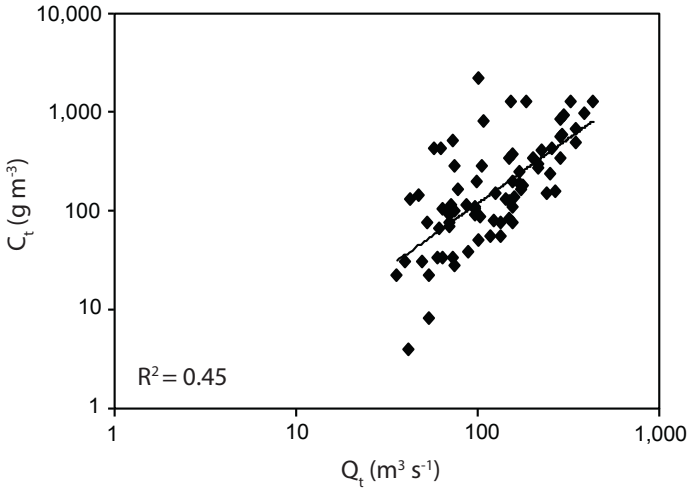

Figure 13. Rating curve calculated for the Wilson River by comparing ln Ct and ln Qt. Data were collected by the USGS at stream gauges that measure daily discharge. β_0, β_1, and ε are -1.23, 1.31, and 0.91, respectively.

Sediment load for the Wilson River was calculated as 240 x 10^3 t yr^{-1}, producing a yield of 480 t km^{-2} yr^{-1}. These values were similar to those calculated by Komar et al. (2004). The 1290 km^2 drainage area, which excludes the Miami River tributary as it is unlikely to contribute significant sediment to core locations, has a calculated load of 620 x 10^3 t yr^{-1}. This value is four times greater than the load calculated from the mean PNW yield (160 x 10^3 t yr^{-1}; Table I).

Compared to other PNW fluvial sediment yields, this value is anomalously high and should thus not be applied to other streams both within the Tillamook Bay watershed and other basins within Oregon. Estimation of load for the three estuaries using the assumed mean PNW yield is a more conservative method and should be considered more accurate until either the USGS collects more sediment concentration samples or an obvious cause of high load within the Wilson River is elucidated.

Appendix II. Constant Rate of Supply model

In addition to the constant initial concentration (CIC) model, Ss were calculated by the constant rate of supply (CRS) model (Appleby and Oldfield 1978; Kolker et al. 2009; Sanchez-Cabeza and Ruiz-Fernández 2012). The CRS model assumes a constant rate of ^{210}Pb flux to the sediment surface from atmospheric fallout. Thus, this method is independent of sedimentation rate as dilutions or concentration of the radionuclide would indicate either increased or slowed sedimentation, respectively (Allen et al. 1993). To determine whether the CRS model's assumptions are met, the inventory of $^{210}Pb_{xS}$ was used to assess the primary pathway by which the radionuclide reaches the wetland surface. ^{210}Pb either reaches the wetland surface through direct atmospheric deposition of radioactively decayed ^{222}Rn or through deposition of lithogenic material of either terrestrial or subtidal origins (Bellucci et al. 2007).

The atmospheric flux of ^{210}Pb is spatially variable (Baskaran 2011), and unfortunately few values are published for the PNW. Nevissi (1985) measured 0.0073 ± 0.004 Bq cm^{-2} yr^{-1} in Seattle WA; Balistrier et al. (1995) and Barnes et al. (1979) have published similar values measured at nearby Lake Sammamish and Lake Washington, respectively. Atmospheric ^{210}Pb flux is correlated to latitude, and this value corresponds well with other measured fluxes within 40 – 50 °N (0.0155 ± 0.0075 Bq cm^{-2} yr^{-1}; Baskaran 2011). Since the Oregon Coast falls within this latitude range, we can assume the steady state inventory of atmospheric ^{210}Pb is 0.24 ± 0.13 Bq cm^{-2}. Inventories of $^{210}Pb_{xS}$ (Q, Bq cm^{-2}) were calculated using eq. 4.

The mean $^{210}Pb_{xS}$ inventory for the estuaries was 0.44 ± 0.09 Bq cm^{-2}. Mean inventories were slightly higher in Tillamook cores ($\bar{Q}$ = 0.53 ± 0.23 Bq cm^{-2}) and lowest in the Youngs Bay cores ($\bar{Q}$ = 0.37 ± 0.25 Bq cm^{-2}); Salmon River cores had an average inventory of 0.41 ± 0.07 Bq

cm^{-2}. Thus, though there may be an additional source of ^{210}Pb to the wetland sediment, the average is in relatively good agreement with the expected $^{210}Pb_{xS}$ inventories if the radionuclide is primarily supplied by atmospheric flux. Moreover, the CRS method is further validated given the coarse sampling resolution (2 cm), which spans multiple years (Bellucci et al. 2007), and an obvious benefit of the CRS model is its detailed history of accretion rate change.

Unlike the CIC method, the CRS model provides a detailed history (< 150 yr) of accumulation rates by calculating ages at each sampling interval (2 cm):

$$Q_z = Q_0 e^{-\lambda t} \quad \text{(eq. 7)}$$

where Q_z is the inventory of $^{210}Pb_{xS}$ below z (Bq cm^{-2}), Q_0 is the total inventory of $^{210}Pb_{xS}$, and t is the age at z (cm). The equation can be rearranged to solve for t at each depth interval:

$$t = -\frac{1}{\lambda} \ln \frac{Q_z}{Q_0} \quad \text{(eq. 8)}$$

and lastly the interval accretion rate (ω) at each z can be calculated:

$$\omega = \frac{z_i - z_{i-1}}{t_i - t_{i-1}} \quad \text{(eq. 9)}$$

Underestimation of the $^{210}Pb_{Xs}$ inventory is an inherent issue associated with the CRS model. As sediments advect downwards and age, $^{210}Pb_{Xs}$ decays eventually falling below current instrument detection limits (3 Bq kg^{-1}). This so called "old date error" (Binford 1990) can however be corrected. Assuming relatively constant sedimentation, the activity at which t is 200 yr (Gonnea 2016) can be calculated by:

$$A_z = A_0 e^{-\lambda t} \quad \text{(eq. 10).}$$

Integration of each $^{210}Pb_{xS}$ plot to the A_{200} depth yields estimates of activities much lower in the profile that fall under the γ-ray spectrometer detection limit. Included in the $^{210}Pb_{Xs}$ inventories, these activities provide more accurate estimates of age and thus interval accretion rate (Figure 14).

Accuracy of each value likely increases with depth as the percent contribution of these estimated values to Q_z increases. Theoretical accretion rates calculated below each profile's detection limit were not included in average Ss.

There exist multiple methods for calculating MARs using the CRS model (Sanchez-Cabeza and Ruiz-Fernández 2012). Sanchez-Cabeza et al. (2000) suggest use of equation:

$$\text{MAR} = \frac{Q_z}{\Delta t \cdot C_z}\left(1 - e^{-\lambda \cdot \Delta t}\right) \qquad \text{(eq. 11)}$$

which can be simplified to:

$$\text{MAR} = \frac{h_i \cdot \rho_i}{\Delta t} \qquad \text{(eq. 12)}$$

where Δt is the formation time (Figure 15). This simplification does not yield different values but slightly over-estimates the associated error. CARs and MDRs were calculated using the depth averaged fraction of C_{org} and 1-LOI, respectively (Table VI).

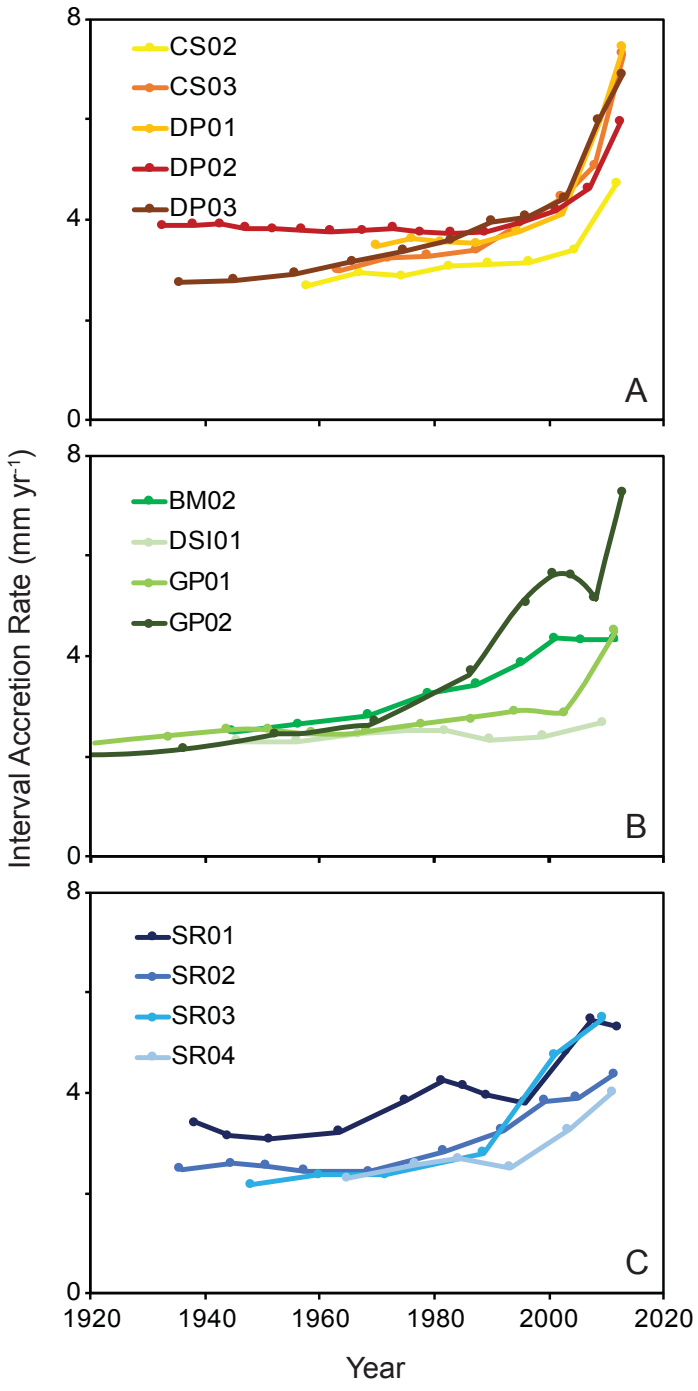

Figure 14. Interval accretion rates calculated by the CRS model and plotted over the last century for each core location. Figures A, B, and C represent data from Youngs Bay, Tillamook Bay, and the Salmon River estuary, respectively.

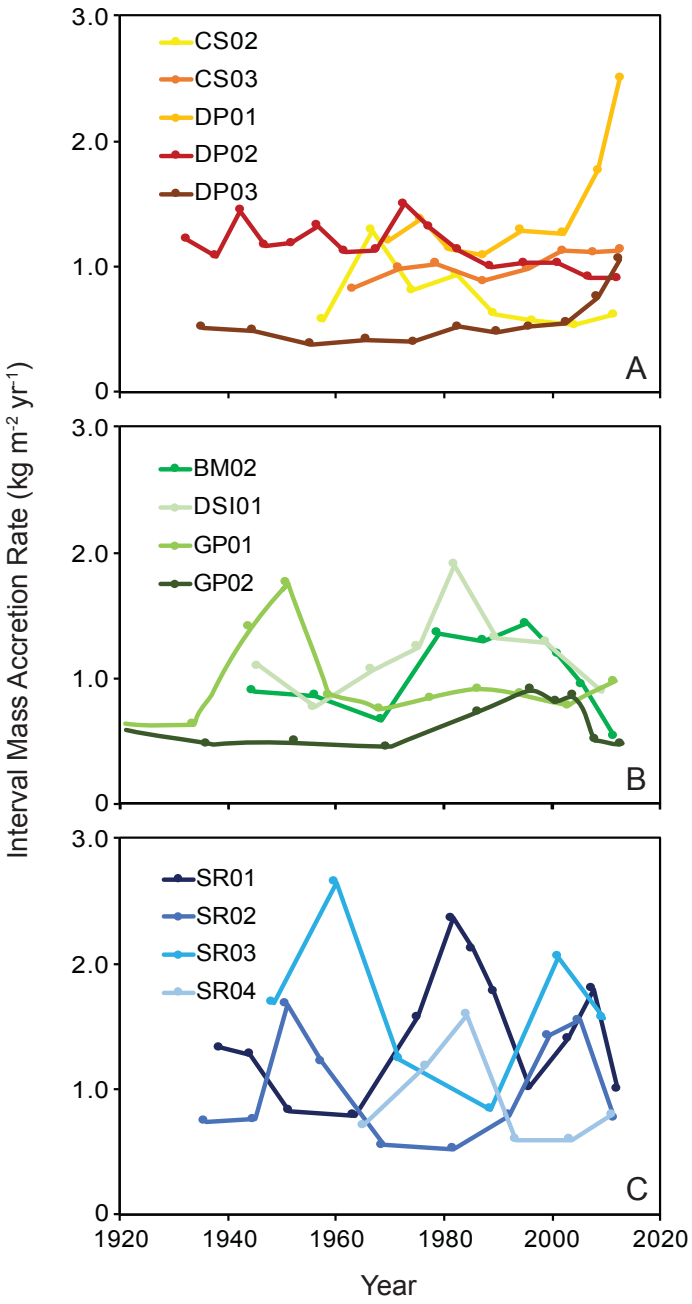

Figure 15. Mass interval accretion rates calculated by the CRS model and plotted over the last century for each core location. Figures A, B, and C represent data from Youngs Bay, Tillamook Bay, and the Salmon River estuary, respectively.

Table VI. Depth averaged Ss, MARs, CARs, and MDRs for each high marsh core from the three estuaries calculated using the CRS model. Mean values are bolded.

Site	S (mm yr^{-1})	MAR (kg m^{-2} yr^{-1})	CAR (g C_{org} m^{-2} yr^{-1})	MDR (g m^{-2} yr^{-1})
Youngs Bay				
CS02	3.2 ± 0.6	0.74 ± 0.26	67 ± 17	680 ± 260
CS03	4.2 ± 1.4	1.0 ± 0.1	110 ± 40	900 ± 90
DP02	4.0 ± 0.6	1.2 ± 0.2	150 ± 20	1000 ± 200
DP03	4.0 ± 1.3	0.55 ± 0.20	120 ± 90	430 ± 110
Mean	**3.9 ± 0.4**	**1.0 ± 0.3**	**110 ± 30**	**750 ± 250**
Tillamook Bay				
BM02	3.5 ± 0.8	1.0 ± 0.3	79 ± 21	930 ± 300
DSI01	2.4 ± 0.1	1.2 ± 0.3	83 ± 20	1100 ± 300
GP01	2.8 ± 0.6	0.94 ± 0.34	79 ± 24	860 ± 320
GP02	3.7 ± 1.8	0.63 ± 0.19	140 ± 100	490 ± 150
Mean	**3.1 ± 0.6**	**0.94 ± 0.24**	**95 ± 30**	**850 ± 260**
Salmon River Estuary				
SR01	4.0 ± 0.8	1.4 ± 0.5	140 ± 40	1300 ± 500
SR02	3.1 ± 0.7	1.0 ± 0.4	120 ± 40	880 ± 400
SR03	3.3 ± 1.4	1.7 ± 0.6	180 ± 50	1500 ± 600
SR04	2.9 ± 0.6	0.92 ± 0.40	130 ± 30	790 ± 370
Mean	**3.3 ± 0.5**	**1.3 ± 0.4**	**140 ± 30**	**1100 ± 300**
Overall Mean	**3.4 ± 0.6**	**1.0 ± 0.3**	**120 ± 30**	**900 ± 300**

Depth averaged Ss calculated by the CIC model were compared to those calculated by the CRS model using a paired t-test (Table VII); there is strong evidence that these two methods yield different Ss (two sided p-value < 7×10^{-5}). Accretion rates calculated using the CRS method were on average 1.1 mm yr^{-1} greater than the Ss calculated using the CIC method. With 95% confidence, a S calculated using the CRS method is between 0.7 and 1.5 mm yr^{-1} greater than a S calculated using the CIC method.

Though neither method's assumptions are obviously invalid and the CRS model is commonly utilized in calculating average Ss for the past century, Ss calculated via the CIC model are preferentially chosen in this study. Examination of the CRS calculated interval accretion rates reveals that all sites have experienced increased Ss over the last century (Figure 15). This result is not in and of itself suspicious as multiple human perturbations to the estuarine system, such as diking, timber harvest, and climate change, may have caused increased wetland sedimentation

within the last half century. However, an apparent increase in sedimentation is remarkably common in studies using the CRS model, causing some to question whether bias inherent to the method may be dictating recent Ss (Gonnea 2016). Correction of the $^{210}Pb_{Xs}$ inventory to ~200 yr weakens the dramatic rise in recent Ss by increasing older Ss. However, lower dry bulk densities towards the sediment surface likely drives the observed increase in recent Ss to a greater degree. As sediments move downwards within the profile, they consolidate and compact resulting in increased dry bulk density with depth. Hence the apparent decrease in linear sedimentation over time. Though this phenomenon is truly occurring and thus should not be corrected for, the CRS model is not an appropriate model for determining mean Ss over the past century.

Depth averaged MARs calculated by the CRS model were, however, not statistically different from those calculated by the CIC model (paired t-test; two sided p-value = 0.4; Table VII). Because the calculation of MARs accounts for changes in bulk density with depth, it is unsurprising that these values are consistent between models. Changes in mass accumulation within the estuaries over the past century can therefore be evaluated using the CRS model.

There was moderate (two-sided p-value = 0.03; Table VII) and strong (two-sided p-value = 0.005; Table VII) evidence that CARs and MDRs were different, respectively. Such a result is surprising since both calculations incorporate changes in density with depth. Given these differences in Ss, CARs, and MDRs calculated by the CRS and CIC models, use of the CRS model should focus on changes in MARs over the past century.

Table VII. Comparison of mean Ss, MARs, CARs, and MDRs for the three estuaries using the two models – CIC and CRS. Low marsh cores, DP01, WY04, BM01, and DSI02, were not included in averages.

	Model	Youngs Bay	Tillamook Bay	Salmon River Estuary	Mean
S ($mm\ yr^{-1}$)	CIC	2.7 ± 0.6	2.2 ± 0.3	2.4 ± 0.7	2.4 ± 0.5
	CRS	3.9 ± 0.4	3.1 ± 0.6	3.3 ± 0.5	3.4 ± 0.6
	Mean	3.3 ± 0.5	2.7 ± 0.7	2.9 ± 0.7	**2.9 ± 0.5**
MAR ($kg\ m^{-2}\ yr^{-1}$)	CIC	0.83 ± 0.33	0.97 ± 0.27	1.0 ± 0.4	0.94 ± 0.31
	CRS	0.87 ± 0.29	0.94 ± 0.24	1.3 ± 0.4	1.0 ± 0.3
	Mean	0.85 ± 0.30	1.0 ± 0.2	1.1 ± 0.4	**1.2 ± 0.9**
CAR ($g\ C_{org}\ m^{-2}\ yr^{-1}$)	CIC	87 ± 35	85 ± 19	110 ± 30	94 ± 33
	CRS	110 ± 30	95 ± 30	140 ± 30	120 ± 30
	Mean	99 ± 33	90 ± 24	130 ± 30	**110 ± 30**
MDR ($g\ m^{-2}\ yr^{-1}$)	CIC	570 ± 240	740 ± 270	700 ± 280	670 ± 250
	CRS	750 ± 250	850 ± 260	1100 ± 300	900 ± 300
	Mean	660 ± 240	790 ± 250	910 ± 370	**790 ± 240**

Appendix III. Bulk density related to organic content

Relatively few global compilations of estuarine characteristics such as wetland vulnerability under sea level rise (e.g., Kirwin et al. 2016) and carbon burial rates (e.g., Chmura et al. 2003; Ouyang and Lee 2014) include examples from the Pacific Northwest. Though these two specific characteristics are discussed above, comparison of our data to that of Morris et al. (2016) is presented here.

Morris et al. (2016) compared dry bulk density and organic content of 5075 samples from 33 different wetlands along the US East, Gulf, and California Coasts. The authors fit empirical power functions, and the ideal mixing model (Adams 1973) in the form of:

$$\rho_{DB} = \frac{1}{\frac{LOI}{k_1}+\frac{1-LOI}{k_2}} \qquad \text{(eq. 13)}$$

where the coefficients k_1 and k_2 are the specific densities of OM and lithogenic matter, respectively. Use of this relationship assumes that the densities of organic and mineral material are constant and that the bulk volume of sediment is simply the addition of their volumes. Though Morris et al. (2016) found the greatest coefficient of determination using the mixing model (R^2 = 0.78 where k_1 and k_2 = 0.085 and 1.99 g cm^{-3}, respectively), they note that the components are not truly additive. Organic material may be either absorbed into clay lattices or adsorbed to mineral surfaces without increasing the volume of the sediment sample (Morris et al. 2016 and references therein).

The relationship between dry bulk density and organic content amongst the Oregon data behaves similarly to other U.S. wetlands (Figure 16). The power law fit to the Oregon data indicates that for the same OM content, Oregon sediment has a slightly higher bulk density than would be predicted for other U.S. wetlands using either the mixing model equation or the power

law equation. Oregon wetland sediment must therefore be particularly susceptible to OM sorption to clay minerals; as a result, this OM may be relatively resistant to remineralization. Inclusion of Oregon wetland data into this relationship will alter any empirical relationship calculated between bulk density and organic content. For instance, the new power law becomes $\rho_{DB} = 3.49\text{LOI}^{-0.80}$ ($R^2 = 0.74$) when both Oregon and the Morris et al. (2016) data are analyzed.

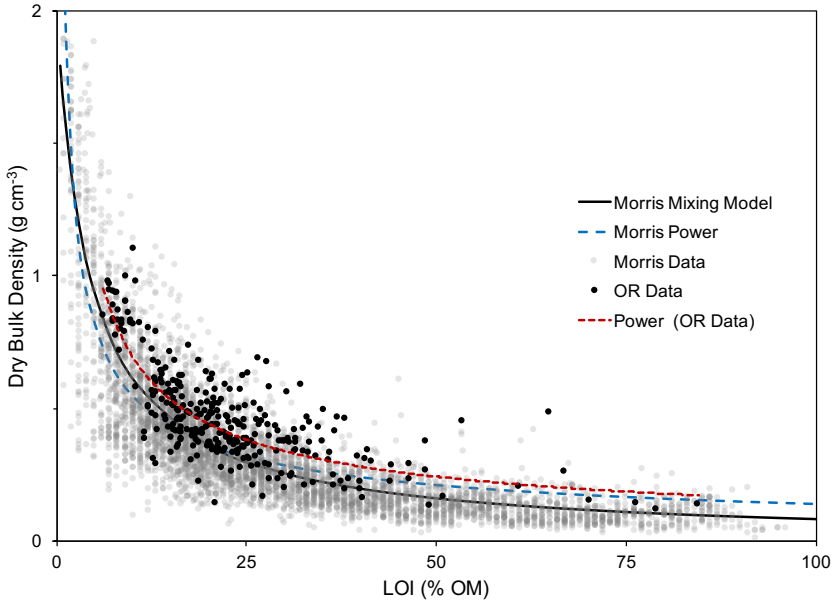

Figure 16. Relationship between dry bulk density and percent OM measured by LOI for samples from this study (black dots, n = 302, wetlands = 3) compared with those presented by Morris et al. (2016; gray dots, n = 5075, wetlands = 33). The black, solid line indicates the mixing model calculated by Morris et al. (2016; $R^2 = 0.78$). The blue, dashed line is the power law calculated by the authors ($R^2 = 0.73$; $\rho_{DB} = 0.14\text{LOI}^{-0.59}$) and the red, dashed line is a best fit power law equation to the Oregon data ($R^2 = 0.58$, $\rho_{DB} = 3.12\text{LOI}^{-0.65}$).

Appendix IV. Sediment characteristics with depth

Table VIII. Sediment dry bulk density (g cm^{-3}) within each 2-cm interval measured throughout the top 50 cm of each core from Youngs Bay, Tillamook Bay, and the Salmon River Estuary. A sampling error caused the top 5 cm of SR03 to be combined and the following 2-cm sampling intervals began and ended on odd depths (e.g., 5-7 cm).

Depth Interval (cm)	Youngs Bay						Tillamook Bay						Salmon River Estuary			
	CS02	CS03	DP01	DP02	DP03	WY04	BM01	BM02	DSI01	DSI02	GP01	GP02	SR01	SR02	SR03	SR04
0-2	0.197	0.233	0.506	0.229	0.231	0.326	0.433	0.182	0.497	0.167	0.323	0.096	0.283	0.266		0.299
2-4	0.223	0.318	0.383	0.262	0.152	0.339	0.580	0.218	0.610	0.140	0.416	0.139	0.317	0.464	0.343	0.235
4-6	0.210	0.333	0.544	0.304	0.203	0.355	0.678	0.264	0.606	0.332	0.289	0.117	0.377	0.385		0.377
6-8	0.207	0.339	0.449	0.317	0.164	0.380	0.829	0.512	0.556	0.472	0.399	0.141	0.463	0.374	0.242	0.447
8-10	0.331	0.435	0.395	0.323	0.135	0.410	0.803	0.565	0.477	0.291	0.358	0.263	0.376	0.291	0.319	0.561
10-12	0.378	0.367	0.305	0.314	0.222	0.406	0.458	0.531	0.491	0.565	0.391	0.484	0.380	0.415	0.377	0.496
12-14	0.369	0.339	0.334	0.332	0.162	0.357	0.563	0.436	0.466	0.372	0.374	0.451	0.468	0.470	0.439	0.461
14-16	0.357	0.428	0.459	0.337	0.194	0.337	0.639	0.473	0.460	0.488	0.571	0.341	0.689	0.451	0.509	0.579
16-18	0.408	0.343	0.755	0.331	0.210	0.359	0.381	0.526	0.518	0.723	0.539	0.430	0.587	0.252	0.493	0.567
18-20	0.368	0.337	0.937	0.314	0.246	0.394	0.456	0.485	0.467	0.559	0.403	0.454	0.384	0.429	0.392 0.375	0.631

Table VIII. Continued.

20-22	0.318	0.376	0.798	0.307	0.224	0.432	0.470	0.635	0.437	0.411	0.445	0.386	0.329	0.370	0.515	0.623
22-24	0.394	0.350	0.838	0.294	0.218	0.445	0.556	0.555	0.467	0.578	0.438	0.384	0.419	0.502	0.638	0.571
24-26	0.394	0.409	0.996	0.289	0.283	0.452	0.817	0.429	0.403	0.412	0.276	0.232	0.564	0.403	0.423	0.587
26-28	0.361	0.430	0.937	0.281	0.235	0.437	0.861	0.611	0.494	0.597	0.435	0.310	0.532	0.412	0.494	0.370
28-30	0.379	0.342	0.716	0.287	0.223	0.403	0.902	0.530	0.538	0.509	0.500	0.335	0.675	0.374	0.507	0.421
30-32	0.407	0.346	0.815	0.328	0.250	0.410	0.969	0.465	0.543	0.516	0.369	0.199	0.373	0.679	0.453	0.478
32-34	0.412	0.346	0.869	0.359	0.312	0.419	0.976	0.429	0.493	0.388	0.523	0.331	0.450	0.424	0.437	0.565
34-36	0.352	0.351	0.831	0.396	0.277	0.497	0.678	0.606	0.587	0.524	0.483	0.306	0.625	0.422	0.477	0.498
36-38	0.416	0.358	0.940	0.392	0.355	0.538	0.668	0.623	0.515	0.598	0.369	0.370	0.518	0.427	0.457	0.498
38-40	0.438	0.392	0.886	0.404	0.364	0.541	0.457	0.594	0.557	0.309	0.518	0.370	0.454	0.487	0.394	0.548
40-42	0.463	0.445	0.775	0.446	0.338	0.530	0.503	0.641	0.587	0.625	0.489	0.344	0.437	0.380	0.412	0.548
42-44	0.414	0.225	0.850	0.442	0.260	0.530	0.467	0.648	0.509	1.101	0.474	0.337	0.474	0.402	0.537	0.524
44-46	0.384	0.484	0.943	0.443	0.307	0.545	0.789	0.790	0.412	0.900	0.512	0.286	0.419	0.344	0.568	0.516

Table VIII. Continued.

46-48	0.399	0.479	0.827	0.460	0.363	0.570	0.977	0.479	0.603	0.821	0.622	0.331	0.712	0.365		0.504
															0.484	
48-50	0.354	0.417	0.819	0.466	0.279	0.578	0.830	0.567	0.420	0.579	0.592	0.311	0.734	0.594		0.524

Table IX. Sediment organic matter content (%OM) within each 2-cm interval measured throughout the top 50 cm of each core from Youngs Bay, Tillamook Bay, and the Salmon River Estuary. A sampling error caused the top 5 cm of SR03 to be combined and the following 2-cm sampling intervals began and ended on odd depths (e.g., 5-7 cm).

Depth Interval (cm)	Youngs Bay						Tillamook Bay						Salmon River Estuary			
	CS02	CS03	DP01	DP02	DP03	WY04	BM01	BM02	DSI01	DSI02	GP01	GP02	SR01	SR02	SR03	SR04
0-2	40.0	38.5	12.2	53.7	73.1	14.0	20.0	41.5	24.1	27.3	31.9	82.0	44.2	48.7		41.5
2-4	36.9	34.1	11.7	49.5	70.1	14.0	13.2	30.5	20.4	20.9	31.5	84.5	26.2	33.0	36.9	46.5
4-6	32.8	33.3	12.8	44.0	60.9	13.8	15.7	26.9	20.2	21.3	27.6	78.9	29.3	31.5		48.6
6-8	25.9	31.4	8.7	40.5	51.0	14.0	9.9	20.7	19.8	13.1	26.2	76.3	37.1	35.1	30.8	33.3
8-10	23.2	27.9	19.1	38.0	49.1	14.0	12.2	18.6	20.6	13.1	24.5	66.8	29.7	46.4	39.7	30.4
10-12	21.1	21.5	17.7	33.8	44.0	13.6	16.0	17.8	21.3	15.7	22.5	64.9	23.8	36.7	30.1	35.2
12-14	18.8	22.0	15.1	31.8	40.3	13.8	12.7	21.3	22.5	20.1	23.5	53.5	22.5	27.5	26.8 24.9	38.0

Table IX. Continued.

14-16	19.9	24.7	16.3	28.6	37.9	14.1	14.0	20.3	19.9	16.1	20.9	41.0	26.6	27.1	27.0	28.1
16-18	18.8	24.0	11.5	29.5	36.6	14.5	18.5	20.5	19.2	12.7	20.8	28.8	32.2	29.8	28.1	22.9
18-20	20.2	23.7	7.8	32.5	36.6	14.8	16.5	17.5	20.1	13.1	21.6	24.7	30.5	34.6	25.8	25.2
20-22	18.7	22.9	8.4	33.0	40.0	14.1	14.3	14.5	20.6	11.7	23.9	25.1	23.8	31.6	21.0	24.6
22-24	18.3	24.7	7.5	37.7	33.9	13.5	15.1	17.2	21.4	16.4	21.0	24.7	19.2	20.7	19.7	24.2
24-26	18.0	22.0	9.2	36.8	26.7	13.2	10.2	14.9	19.3	17.9	21.8	29.3	15.8	22.2	25.4	22.3
26-28	16.1	19.8	8.0	34.7	28.1	13.1	9.5	13.0	15.9	15.9	24.2	40.7	21.8	29.2	30.4	18.3
28-30	16.4	20.7	8.3	33.4	37.5	13.7	9.2	13.9	15.5	16.7	23.2	32.5	27.8	30.1	20.0	15.6
30-32	16.5	21.5	8.6	29.5	31.0	13.2	7.0	16.8	16.5	14.7	22.9	30.0	23.0	18.7	18.3	17.5
32-34	15.7	22.3	8.1	25.0	25.2	13.7	6.8	16.4	18.6	15.1	20.0	36.0	23.6	23.1	23.6	15.6
34-36	15.9	21.3	8.6	20.8	24.2	13.9	12.8	13.8	16.1	15.6	20.4	35.8	20.6	32.6	26.3	14.9
36-38	15.5	20.4	7.6	21.7	26.0	13.5	13.5	16.7	15.4	13.2	24.0	33.3	26.0	29.3	22.5	14.4
38-40	15.4	23.0	7.4	22.7	25.2	11.9	14.5	13.9	14.4	12.7	21.5	30.8	26.4	24.4	20.6	14.4

Table IX. Continued.

40-42	16.1	22.7	7.8	18.0	21.9	11.1	12.1	13.7	14.7	14.0	19.6	31.5	24.1	35.7		13.2
															28.5	
42-44	16.1	18.8	6.2	18.0	23.2	10.2	18.6	14.5	15.4	10.2	18.9	29.1	19.0	29.8		12.0
															41.5	
44-46	16.5	17.3	7.0	16.6	24.7	9.3	9.0	13.1	17.9	9.2	17.7	28.1	13.2	30.9		11.6
															23.8	
46-48	18.3	17.7	7.6	15.3	23.4	9.1	10.4	12.7	15.5	10.9	16.3	26.9	14.9	24.2		10.5
															12.8	
48-50	18.1	17.3	9.8	15.1	25.7	9.7	8.2	14.9	18.4	10.6	16.2	25.5	17.4	16.7		9.7

Table X. Sediment organic carbon content ($\%C_{org}$) within each 2-cm interval measured throughout the top 50 cm of each core from Youngs Bay, Tillamook Bay, and the Salmon River Estuary. A sampling error caused the top 5 cm of SR03 to be combined and the following 2-cm sampling intervals began and ended on odd depths (e.g., 5-7 cm).

Depth Interval (cm)	Youngs Bay						Tillamook Bay						Salmon River Estuary			
	CS02	CS03	DP01	DP02	DP03	WY04	BM01	BM02	DSI01	DSI02	GP01	GP02	SR01	SR02	SR03	SR04
0-2	14.9	14.2	3.8	21.6	32.3	4.5	6.6	15.6	8.2	9.4	11.4	37.7	16.9	19.0		15.6
2-4	13.5	12.3	3.7	19.5	30.6	4.5	4.2	10.8	6.8	7.0	11.2	39.3	9.0	11.8	13.5	18.0
4-6	11.7	12.0	4.1	16.8	25.4	4.4	5.0	9.3	6.7	7.1	9.6	35.8	10.3	11.2		19.0
6-8	8.9	11.2	2.7	15.1	20.2	4.5	3.1	6.9	6.6	4.1	9.0	34.2	13.6	12.7	10.9 14.8	12.0

T**able X.** Continued

8-10	7.9	9.7	6.3	14.0	19.2	4.5	3.8	6.1	6.9	4.2	8.4	28.7	10.5	17.9	10.6	10.7
10-12	7.0	7.2	5.8	12.2	16.8	4.3	5.2	5.8	7.1	5.0	7.6	27.6	8.1	13.5	9.3	12.8
12-14	6.2	7.4	4.8	11.3	15.1	4.4	4.0	7.1	7.6	6.7	7.9	21.4	7.6	9.6	8.5	14.0
14-16	6.6	8.4	5.3	10.0	14.0	4.5	4.5	6.7	6.6	5.2	7.0	15.4	9.2	9.4	9.3	9.8
16-18	6.2	8.2	3.6	10.4	13.4	4.6	6.1	6.8	6.3	4.0	6.9	10.1	11.5	10.5	9.8	7.7
18-20	6.7	8.0	2.4	11.6	13.4	4.7	5.3	5.7	6.7	4.2	7.2	8.4	10.8	12.5	8.9	8.6
20-22	6.1	7.7	2.6	11.8	14.9	4.5	4.6	4.6	6.9	3.7	8.1	8.6	8.1	11.2	7.0	8.4
22-24	6.0	8.4	2.3	13.9	12.2	4.3	4.9	5.6	7.2	5.3	7.0	8.4	6.4	6.9	6.5	8.3
24-26	5.9	7.4	2.9	13.5	9.2	4.2	3.2	4.8	6.4	5.9	7.3	10.3	5.1	7.5	8.7	7.5
26-28	5.2	6.6	2.5	12.6	9.8	4.1	2.9	4.1	5.2	5.1	8.2	15.3	7.3	10.2	10.8	6.0
28-30	5.3	6.9	2.6	12.0	13.8	4.4	2.8	4.4	5.0	5.4	7.8	11.6	9.7	10.6	6.6	5.0
30-32	5.4	7.2	2.7	10.3	11.0	4.2	2.1	5.5	5.4	4.7	7.7	10.6	7.8	6.2	6.0	5.7
32-34	5.1	7.5	2.5	8.5	8.6	4.4	2.1	5.3	6.1	4.9	6.6	13.1	8.0	7.8	8.0	5.0

Table X. Continued.

34-36	5.1	7.1	2.7	6.9	8.2	4.4	4.0	4.4	5.2	5.0	6.8	13.0	6.8	11.7	9.1	4.8
36-38	5.0	6.8	2.3	7.3	9.0	4.3	4.3	5.4	4.9	4.2	8.1	12.0	8.9	10.3	7.6	4.6
38-40	5.0	7.8	2.3	7.6	8.6	3.8	4.6	4.4	4.6	4.0	7.2	10.9	9.1	8.3	6.9	4.6
40-42	5.2	7.7	2.4	5.9	7.3	3.5	3.8	4.4	4.7	4.5	6.5	11.2	8.2	13.0	10.0	4.2
42-44	5.2	6.2	1.9	5.9	7.8	3.2	6.1	4.6	5.0	3.2	6.2	10.2	6.3	10.5	15.6	3.8
44-46	5.4	5.6	2.1	5.4	8.4	2.9	2.8	4.2	5.9	2.8	5.8	9.8	4.2	10.9	8.1	3.6
46-48	6.0	5.8	2.3	4.9	7.9	2.8	3.3	4.0	5.0	3.4	5.3	9.3	4.8	8.2	4.1	3.3
48-50	5.9	5.6	3.0	4.9	8.8	3.0	2.5	4.8	6.0	3.3	5.2	8.7	5.7	5.4		3.0